AD-A080 603 OHIO STATE UNIV COLUMBUS ELECTROSCIENCE LAB F/G 9/5
ANALYSIS OF ELECTRICALLY THIN, DIELECTRIC LOADED CAVITY BACKED --ETC(U)
DEC 79 E H NEWMAN DAAG29-76-G-0331
UNCLASSIFIED ESL-4569-11 ARO-14012.6-EL NL

| OF |
AD
A080603

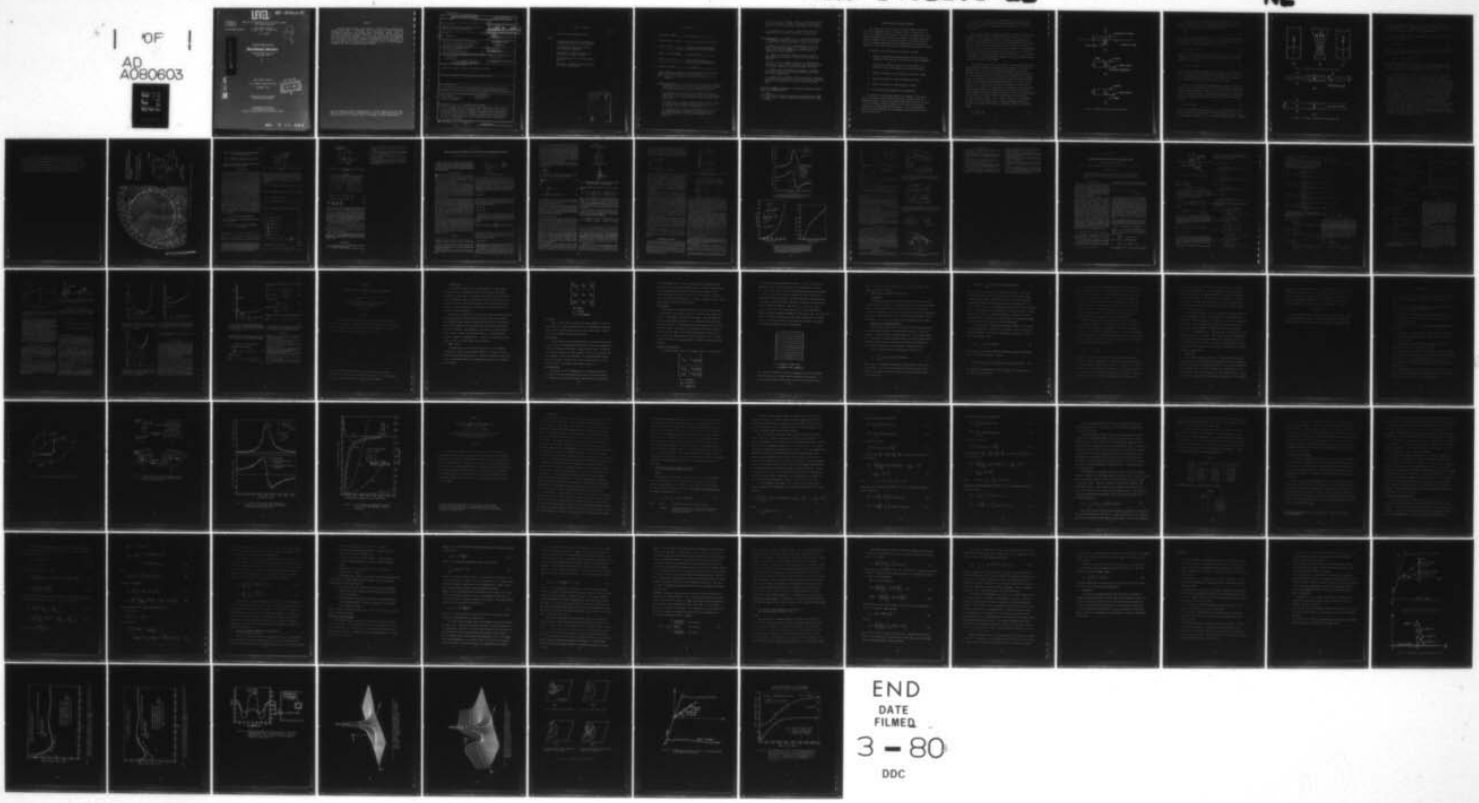

END
DATE FILMED
3 - 80
DDC

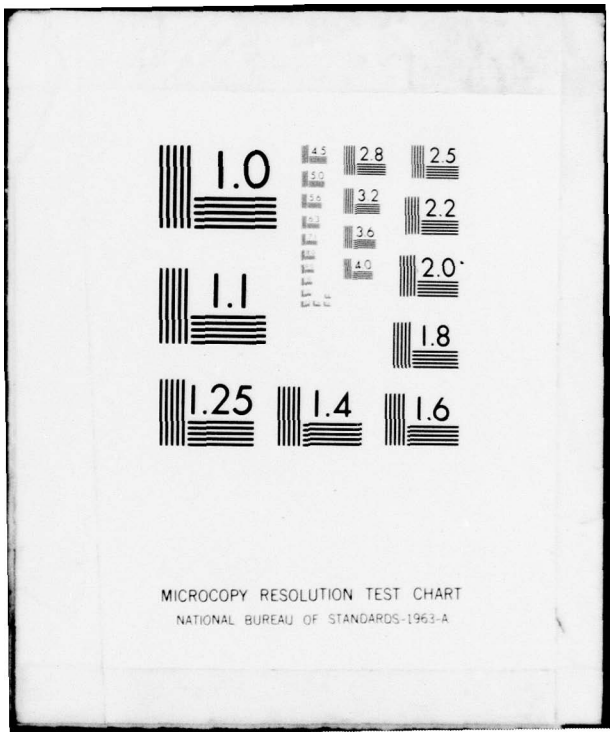
1.0
1.1
1.25
1.4
1.6
1.8
2.0
2.2
2.5
2.8
3.2
3.6
4.0
4.5
5.0
5.6
MICROCOPY RESOLUTION TEST CHART
NATIONAL BUREAU OF STANDARDS-1963-A

LEVEL II

ARO 14012.6-EL

OSU

The Ohio State University

ANALYSIS OF ELECTRICALLY THIN, DIELECTRIC LOADED CAVITY BACKED RADIATOR

FINAL REPORT 784569-11
24 Sept. 1976 - 23 Sept. 1979

E. H. Newman

12

The Ohio State University

ElectroScience Laboratory

Department of Electrical Engineering
Columbus, Ohio 43212

FINAL REPORT 784569-11

Grant Number DAAG29-76-G-0331

December 1979

APPROVED FOR PUBLIC RELEASE:
DISTRIBUTION UNLIMITED.

Department of the Army
U. S. Army Research Office
Research Triangle Park, North Carolina 27709

NOTICES

When Government drawings, specifications, or other data are used for any purpose other than in connection with a definitely related Government procurement operation, the United States Government thereby incurs no responsibility nor any obligation whatsoever, and the fact that the Government may have formulated, furnished, or in any way supplied the said drawings, specifications, or other data, is not to be regarded by implication or otherwise as in any manner licensing the holder or any other person or corporation, or conveying any rights or permission to manufacture, use, or sell any patented invention that may in any way be related thereto.

The view, opinions, and/or findings contained in this report are those of the author(s) and should not be construed as an official department of the army position, policy, or dicision, unless so designated by other documentation.

UNCLASSIFIED

SECURITY CLASSIFICATION OF THIS PAGE *(When Data Entered)*

REPORT DOCUMENTATION PAGE

READ INSTRUCTIONS BEFORE COMPLETING FORM

1. REPORT NUMBER	2. GOVT ACCESSION NO. 3. RECIPIENT'S CATALOG NUMBER
4. TITLE *(and Subtitle)*	5. TYPE OF REPORT & PERIOD COVERED
ANALYSIS OF ELECTRICALLY THIN, DIELECTRIC LOADED CAVITY BACKED RADIATOR	Final Report 24 Sep 1976 - 23 Sep 1979
	6. PERFORMING ORG. REPORT NUMBER ESL-4569-11 ESL-784569-11
7. AUTHOR(s)	8. CONTRACT OR GRANT NUMBER(s)
E. H. Newman	Grant No. DAAG29-76-G-0331
9. PERFORMING ORGANIZATION NAME AND ADDRESS The Ohio State University ElectroScience Laboratory, Department of Electrical Engineering, Columbus, Ohio 43212	10. PROGRAM ELEMENT, PROJECT, TASK AREA & WORK UNIT NUMBERS 12 76
11. CONTROLLING OFFICE NAME AND ADDRESS Department of the Army U. S. Army Research Office Research Triangle Park, North Carolina 27709	12. REPORT DATE December 1979
	13. NUMBER OF PAGES 72
14. MONITORING AGENCY NAME & ADDRESS *(if different from Controlling Office)* 18 ARO 19 14012.6-EL	15. SECURITY CLASS. *(of this report)* Unclassified
	15a. DECLASSIFICATION/DOWNGRADING SCHEDULE

16. DISTRIBUTION STATEMENT *(of this Report)*

Approved for public release; distribution unlimited.

17. DISTRIBUTION STATEMENT *(of the abstract entered in Block 20, if different from Report)*

18. SUPPLEMENTARY NOTES

The view, opinions, and/or findings contained in this report are those of the author(s) and should not be construed as an official department of the army position, policy, or decision unless so designated by other documentation.

19. KEY WORDS *(Continue on reverse side if necessary and identify by block number)*

Moment methods
Surface patch modeling
Microstrip antennas
Cavity antennas
Dielectrics

20. ABSTRACT *(Continue on reverse side if necessary and identify by block number)*

This summary describes the work on ARO Grant Number DAAG29-76-G-0331 from 24 September 1976 to 23 September 1979. The purpose of this grant is to develop the basic theory, algorithms and computational techniques to analyze the electrically thin, dielectric loaded, cavity backed radiator. The overall approach will be to develop techniques which are applicable to a wide class of geometries, and to apply these general techniques to this specific antenna.

DD FORM 1 JAN 73 1473 EDITION OF 1 NOV 65 IS OBSOLETE

UNCLASSIFIED

SECURITY CLASSIFICATION OF THIS PAGE *(When Data Entered)*

JOB

402 251

TABLE OF CONTENTS

FINAL REPORT

1. ARO PROPOSAL NUMBER: 05228-55-00

2. PERIOD COVERED BY REPORT: Sept. 24, 1976 to Sept. 23, 1979

3. TITLE OF PROPOSAL: Analysis of Electrically Thin, Dielectric Loaded Cavity Backed Radiator

4. CONTRACT OR GRANT NUMBER: DAAG29-76-G-0331

5. NAME OF INSTITUTION: Ohio State University ElectroScience Laboratory

6. AUTHOR(S) OF REPORT: E. H. Newman

7. LIST OF MANUSCRIPTS SUBMITTED OR PUBLISHED UNDER ARO SPONSORSHIP DURING THIS PERIOD, INCLUDING JOURNAL REFERENCES:
Note: Copies of the journal publications are included in the appendices.

Journal publications J. H. Richmond, D. M. Pozar and E. H. Newman, "Rigorour Near Zone Field Expressions for Rectangular Sinusoidal Surface Monopole," IEEE Trans. on Antennas and Propagation, Vol. AP-26, May 1978, pp. 509-510 (see Appendix A).

E. H. Newman and D. M. Pozar, "Electromagnetic Modeling of Composite Wire and Surface Geometries," IEEE Trans. on Antennas and Propagation, Vol. AP-26, November 1979, pp. 784-789 (see Appendix B).

D. M. Pozar and E. H. Newman, "Near Fields of a Vector Electric Line Source Near the Edge of a Wedge," Radio Science, Vol. 14, May-June 1979, pp. 397-403 (see Appendix C).

E. H. Newman and D. M. Pozar, "Considerations for Efficient Wire/Surface Modeling," Scheduled for publication in the Jan. 1980 IEEE Trans. on Antennas and Propagation (see Appendix D).

D. M. Pozar and E. H. Newman, "Analysis of a Monopole Mounted Near or at the Edge of a Wedge," Submitted for publication in the IEEE Trans. on Antennas and Propagation (see Appendix E).

E. H. Newman and P. Tulyathan, "A Moment Method Microstrip Antenna Analysis Technique," Manuscript in preparation.

Oral Presentations E. H. Newman and C. H. Walter,"Recent Advances in the Method of Moments," Presented at the 1977 Symposium on Antenna Applications, Monticello, Illinois, April 1977.

E H. Newman and D. M. Pozar, "Electromagnetic Modeling of Composite Wire/Surface Geometries," Presented at the 1977 International IEEE-APS Symposium and USN/URSI Meeting, Stanford University, June 1977.

E. H. Newman, "Surface Patch Computer Code," Workshop on Moment Methods, University of Syracuse, Syracuse New York, June 1978.

D. M. Pozar and E. H. Newman, "Analysis of a Monopole Near the Edge of a Half Plane," Presented at the 1979 International IEEE APS/URSI Symposium, Seattle, Washington, June 1979.

E. H. Newman, "Microstrip Analysis Techniques," Presented at the 48th Interservice Antenna Group Meeting, Point Mugu California, February 1979.

E. H. Newman and P. Tulyathan, "Microstrip Analysis Technique," Presented at the Workshop on Printed Circuit Antenna Technology, New Mexico St University, Las Cruces, New Mexico, October 1979.

8. SCIENTIFIC PERSONNEL SUPPORTED BY THIS PROJECT AND DEGREES AWARDED DURING THIS REPORTING PERIOD:

E. H. Newman
D. M. Pozar (PhD in Electrical Engineering anticipated March 1980)
P. Tulyathan (PhD in Electrical Engineering anticipated June 1980)
C. H. Walter

BRIEF OUTLINE OF RESEARCH FINDINGS

This summary describes the work on ARO Grant Number DAAG29-76-G-0331 from 24 September 1976 to 23 September 1979. The purpose of this grant is to develop the basic theory, algorithms and computational techniques to analyze the electrically thin, dielectric loaded, cavity backed radiator, commonly called a microstrip antenna. The overall approach will be to develop techniques which are applicable to a wide class of geometries, and to apply these general techniques to this specific antenna.

Our approach can be divided into six steps as follows:

1. Develop a general purpose moment method code for analyzing geometries involving wires, plates and wire plate attachments.

2. Show that this general purpose code is applicable to the electrically thin cavity antenna, or microstrip antenna.

3. Adapt the technique to treat patches of "arbitrary" shape.

4. Adapt the technique to treat attachments near edges.

5. Adapt the technique to treat dielectric loading.

6. Verify accuracy by comparison with measurements.

At present all steps except number 4 are complete. Thus, we are able to analyze coax fed microstrip antennas of rectangular and non-rectangular shape. Although considerable effort was applied to the study of wires attached to edges of plates, we do not have a satisfactory technique for treating edge fed microstrips. Our current techniques predict resonant frequency, but not impedance level accurately for the edge fed microstrips.

The appendices reproduce our journal publications resulting from this research. The application of these techniques to the microstrip antenna is the subject of a manuscript now in preparation. It is summarized below.

Most previous work on microstrip antennas can be divided into three categories. First, there are the transmission line models, where the unknowns are the propagation constant, characteristic impedance, and loads on an equivalent transmission line which approximates the microstrip antenna. Second, there are the modal solutions, where the unknowns are the distribution of cavity modes in the cavity formed by the region between the microstrip patch and the ground plane. By contrast, in our solution the unknown is the current flowing on the microstrip patch. This current is determined by using the method of moments to solve an integral equation in which the current is the unknown.

The basic building block in our solution is a moment-method surface-patch modeling technique for analyzing bodies composed of wires and conducting plates. First it will be shown how the basic surface-patch technique is applied to the air-dielectric microstrip antenna of Figure 1a. The antenna consists of a plate or patch a distance T above a ground plane. The antenna is coaxially fed with the center conductor extending beyond the ground plane and contacting the top patch. In Figure 1b the ground plane is removed and the images of the top patch and the center conductor are inserted. The coax aperture is modeled by a voltage source. Previous experience by this author and others indicates that the coax center conductor need not be modeled as a metallic wire, but can be modeled rather simply as a constant current filament where for convenience a current of one amp is used. This is shown in Figure 1c. The geoemtry of Figure 1c can be analyzed with a surface-patch moment-method code. Briefly, the current on the patches is expanded in terms of N expansion modes:

$$\underline{J}_S = \sum_{n=1}^{N} K_n \underline{J}_n. \qquad (1)$$

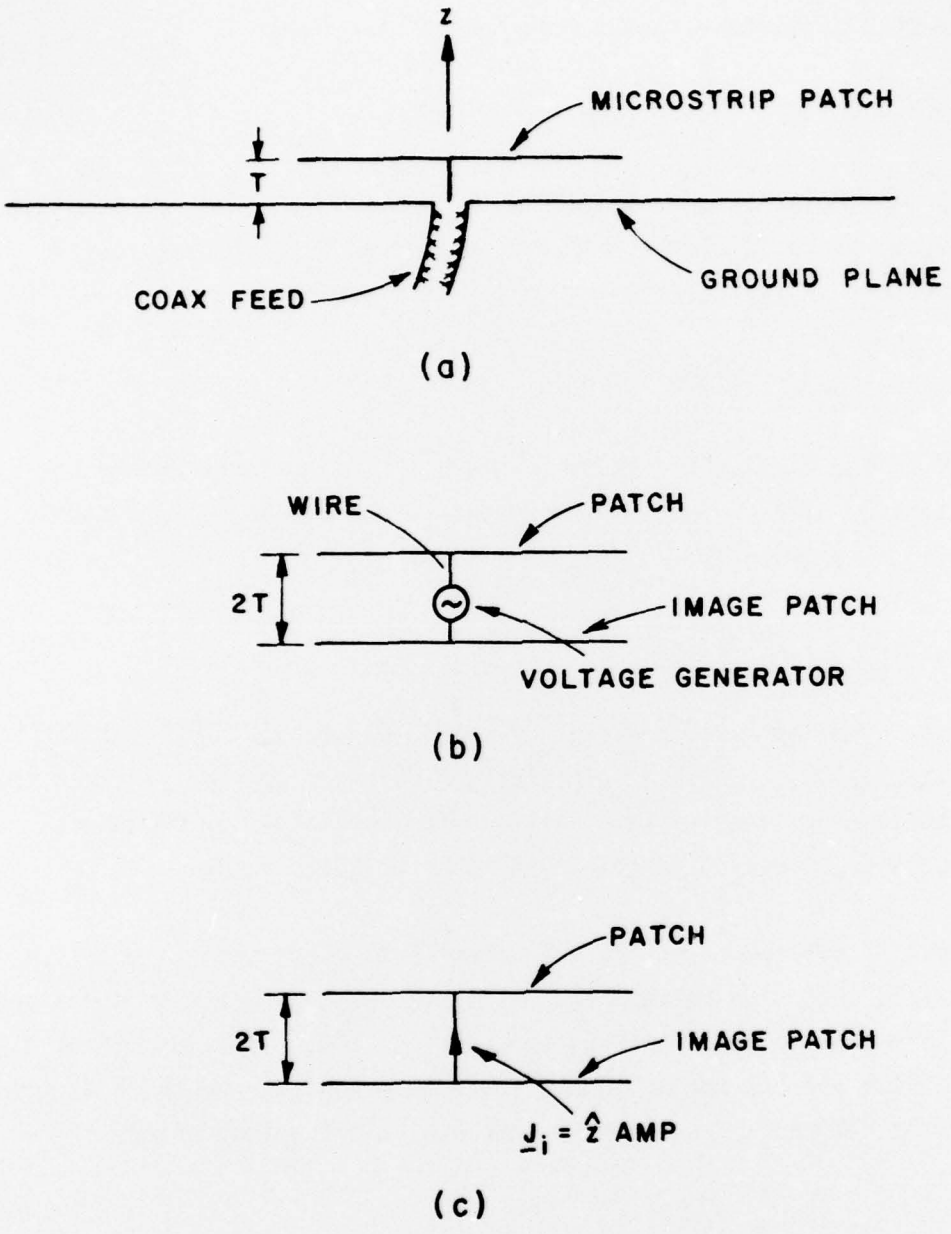

Figure 1. Models for the microstrip antenna.

Typical rectangular surface patch current expansion or testing modes are shown in Figure 2a. The moment-method solution results in a system of simultaneous linear equations of the form

$$[Z]\, I = V \tag{2}$$

where $[Z]$ is the NxN impedance matrix, I is a column vector containing the N expansion coefficients in Equation (1) and V is the excitation column vector. A typical element in $[Z]$ is given by

$$Z_{mn} = - \int_n \underline{J}_n \cdot \underline{E}^m \, ds \tag{3}$$

where $\underline{E}^m$ is the free space fields of the m^{th} testing function and the integration is over the surface of the n^{th} expansion mode. A typical element of V is given by

$$V_m = \int_i \underline{J}_i \cdot \underline{E}^m \, ds \tag{4}$$

where $\underline{J}_i$ is the impressed one-amp current in Figure 1c. Application of this technique is in principle straight-forward, however, in practice it is challenging since certain terms in the moment method impedance matrix need to be evaluated to within about 0.1% accuracy.

Next it will be shown how the moment method solution is modified by the dielectric slab between the microstrip patch and the ground plane. Figure 3a shows the model of Figure 1c, but with the addition of the dielectric slab and its image. Using the volume equivalence theorem, the slab may be removed and replaced by the equivalent volume polarization currents

$$\underline{J}_v = j\omega(\varepsilon - \varepsilon_o)\underline{E} \tag{5}$$

where ε is the permittivity of the slab, ε_o is the permittivity of free space, and $\underline{E}$ is the actual electric field intensity in the slab. This is illustrated in Figure 3b. $\underline{J}_v$ is, of course, unknown since $\underline{E}$ is unknown.

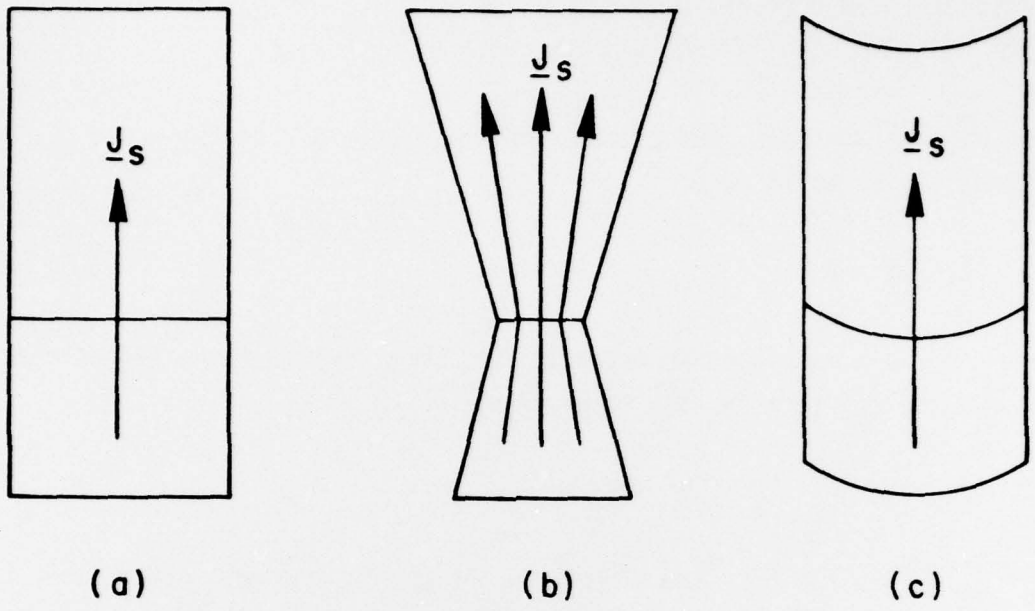

Figure 2. Surface patch expansion and test modes.

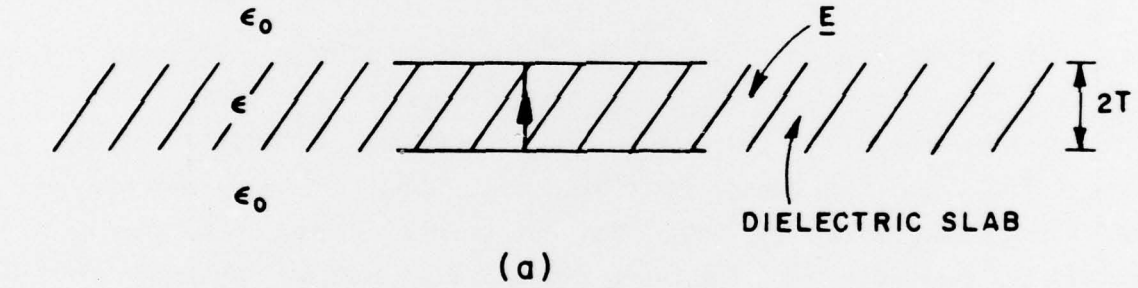

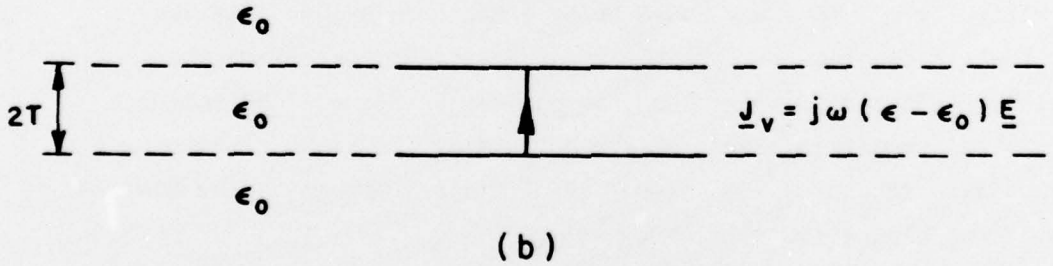

Figure 3. Microstrip antenna with dielectric slab.

We have had previous experience in modifying moment-method solutions to account for dielectric inhomogeneities where $\underline{J}_v$ and $\underline{J}_s$ are considered either as independent unknowns or as dependent unknowns.

Here we consider them to be dependent unknowns. In this case Equation (2) is modified to

$$\left[Z+\Delta Z\right] I = V \tag{6}$$

where ΔZ is a matrix which accounts for the presence of the dielectric slab. A typical term in $\left[\Delta Z\right]$ is given by

$$\Delta Z_{mn} = - j\omega(\epsilon-\epsilon_o) \int_v \underline{E}_d^n \cdot \underline{E}^m \, dv \tag{7}$$

where $\underline{E}_d^n$ is the field of the n^{th} expansion mode in the presence of the dielectric slab, E^m is still the free space field of the m^{th} test mode, and the integral is over the volume of the dielectric slab.

If the exact Green's function for the slab is used in evaluating $\underline{E}_d^n$, then the presence of the slab is handled exactly. Unfortunately, the Green's function for the slab involves the Sommerfeld integrals which are difficult and time consuming to evaluate. Thus, to have a numerically efficient technique for evaluating the ΔZ matrix we need a much simpler method for evaluating $\underline{E}_d^n$. The first approximation used was that only the $\hat{z}$ the component of $\underline{E}_d^n$ would be significant in the slab. Next, previous work suggested that $\hat{z} \cdot \underline{E}_d^n$ in the slab could be reasonably approximated by the $\hat{z}$ component of the fields radiated by $\underline{J}_n$ in a homogeneous medium of permittivity ϵ. This was found to be a reasonable approximation except that it ignores the fact that, for a surface current on the surface of a slab, the normal component of the $\underline{D}$ field in air will be somewhat less than the normal component of the $\underline{D}$ field in the slab. This effect was taken into account using the method of dielectric images and considering the fields to be quasi-static in the slab.

Figure 4 shows a comparison of measured and calculated input impedance for a coaxially-fed rectangular microstrip. Although the details were not mentioned above, losses in the dielectric and in the finitely conducting patches were included in the calculations, and have a significant effect on the bandwidth and the impedance level. Non-rectangular plates can be treated using the modes of Figure 2b.

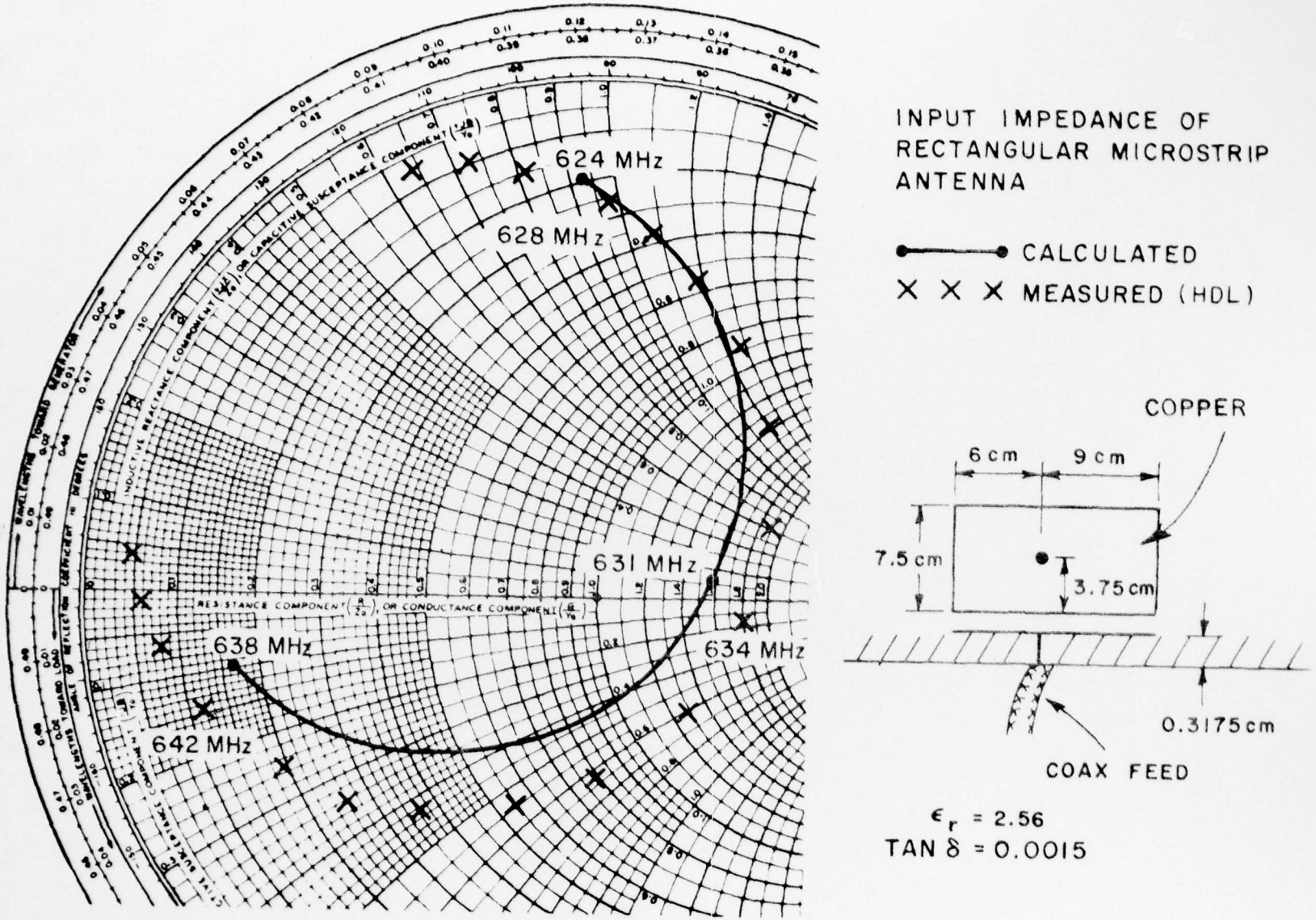

Figure 4. Input impedance of rectangular microstrip antenna.

APPENDIX A

Rigorous Near-Zone Field Expressions for Rectangular Sinusoidal Surface Monopole

JACK H. RICHMOND, SENIOR MEMBER, IEEE, D. M. POZAR, AND EDWARD H. NEWMAN, MEMBER, IEEE

Abstract—The near-zone fields of the sinusoidal surface monopole are presented in terms of exponential integrals.

I. INTRODUCTION

It is widely known that a sinusoidal electric line source with arbitrary length has simple rigorous near-zone field expressions [1]. Furthermore, this has been used with considerable advantage in moment-method solutions for thin-wire antennas and scatterers with arbitrary shape [2]–[4]. In moment-method solutions for sheet-metal antennas and scatterers, it is advantageous to use surface dipoles (instead of thin-wire dipoles) for expanding the unknown surface current density in a basis set [5]. A great deal of computational expense can be avoided by selecting a surface current mode with near-zone fields expressible as a finite series of tabulated functions. Only the sinusoidal surface current distribution is known to have this important property. The field of the sinusoidal dipole may be obtained by summing the fields of two sinusoidal monopoles.

Using the field expressions peresented here, computer subroutines have been developed for the fields of sinusoidal surface monopoles and dipoles. These algorithms are found to be efficient and stable, even when the observation point is near or on the source. Furthermore, the calculated fields satisfy all the appropriate boundary conditions at the source. When the distance to the observation point is not too small, the fields may be obtained readily with numerical integration. In moment-method applications, however, the observer is often on or extremely close to the source where the numerical approach is difficult.

II. NEAR-ZONE FIELD EXPRESSIONS

Consider a time-harmonic source with the following electric surface current density:

$$J_s = \frac{\hat{z}\gamma[I_1 \sinh \gamma(z_2 - z) + I_2 \sinh \gamma(z - z_1)] \cosh \gamma y}{2 \sinh(\gamma h) \sinh(\gamma w)} \tag{1}$$

The time dependence $e^{j\omega t}$ is understood. As illustrated in Fig. 1, this source lies in the yz plane in the region $-w \le y \le w$ and $z_1 \le z \le z_2$. This is a planar rectangular source with edge dimensions $2w$ and h, where $h = z_2 - z_1$. The constants I_1 and I_2 denote the terminal currents in amperes at z_1 and z_2.

Manuscript received February 5, 1977; revised July 8, 1977. This work was supported in part between the United States Army Research Office, Research Triangle Park, North Carolina, and The Ohio State University Research Foundation under Contract DAAG29-76-C-0331.

The authors are with the Department of Electrical Engineering, Ohio State ElectroScience Laboratory, Columbus, OH 43212.

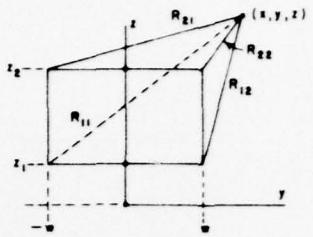

Fig. 1. Geometry of rectangular surface monopole and observation point.

respectively. Let this rectangular surface monopole radiate in a homogeneous conducting medium with intrinsic impedance η and propagation constant γ. By integrating (with respect to y') the fields of the sinusoidal line source, we obtain the following expressions for the fields of the sinusoidal surface monopole:

$$E_x(x, y, z) = j\eta C[(I_2 S_2 - I_1 S_1) \sinh \gamma h + I_{12} F_1 + I_{21} F_2] \tag{2}$$

$$E_y(x, y, z) = \eta C[(I_2 T_2 - I_1 T_1) \sinh \gamma h + I_{12} G_1 + I_{21} G_2] \tag{3}$$

$$E_z(x, y, z) = 2\eta C(I_{12} V_1 + I_{21} V_2) \tag{4}$$

$$H_x(x, y, z) = C[(I_2 G_2 - I_1 G_1) \sinh \gamma h + I_{12} T_1 + I_{21} T_2] \tag{5}$$

$$H_y(x, y, z) = jC[(I_1 F_1 - I_2 F_2) \sinh \gamma h - I_{12} S_1 - I_{21} S_2] \tag{6}$$

$$H_z(x, y, z) = 0 \tag{7}$$

$$C = \gamma/(32\pi \sinh \gamma h \sinh \gamma w) \tag{8}$$

$$I_{12} = I_1 \cosh \gamma h - I_2 \tag{9}$$

$$I_{21} = I_2 \cosh \gamma h - I_1 \tag{10}$$

$$F_n = \sum klmE(k, l, m, n) \tag{11}$$

$$G_n = \sum mE(k, l, m, n) \tag{12}$$

$$S_n = \sum klE(k, l, m, n) \tag{13}$$

$$T_n = -2E(0, 1, 0, n) - 2E(0, -1, 0, n) + \sum E(k, l, m, n) \tag{14}$$

$$V_n = E(0, 1, 0, n) - E(0, -1, 0, n) \tag{15}$$

$$E(k, l, m, n) = e^{jk\gamma x} e^{l\gamma y} e^{m\gamma(z - z_n)} \int_a^b \frac{e^{-\gamma u}\, du}{u} \tag{16}$$

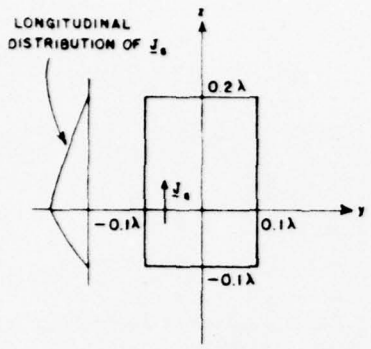

Fig. 2. Geometry of rectangular surface dipole with fields given in Table I.

TABLE I
ELECTRIC FIELD STRENGTH IN V/M FOR SURFACE DIPOLE IN FIG. 2 ALONG LINE (x, y, z) = (x, 0.05λ, 0.1λ)

x/λ	E_x		E_y		E_z	
10^{-9}	814.490	∠-90.0°	231.251	∠-90.4°	137.650	∠152.8°
0.25	35.291	∠-100.3	6.068	∠-101.8	91.210	∠138.2
0.50	8.081	∠-149.0	.778	∠-150.7	56.969	∠67.5
0.75	3.513	∠139.4	.230	∠138.1	40.084	∠-15.2
1.00	1.963	∠59.3	.097	∠58.3	30.677	∠-101.5

$$a = R_{n1} + jkx + l(y - y_1) + m(z - z_n) \tag{17}$$

$$b = R_{n2} + jkx + l(y - y_2) + m(z - z_n) \tag{18}$$

$$\sum = \sum_{k=-1}^{1} \sum_{l=-1}^{1} \sum_{m=-1}^{1} \tag{19}$$

As indicated in Fig. 1, R_{n1} and R_{n2} denote the distance from a corner of the source to the observation point. In (17) and (18), $y_1 = -w$ and $y_2 = w$. For the exponential integral in (16), subroutine EXPJ is available [2], [3]. In the summations, the indices k, l, and m take on only the values -1 and $+1$, so there are eight terms altogether in the triple sum. The expression for E_y is correct only if x differs from zero. When x vanishes, however, the correct field may still be obtained from (3) with any suitably small value of x such as $x = w/10^6$.

The sinusoidal monopole has line charges on the edges at $z = z_1$ and $z = z_2$, but they will disappear when another monopole is connected to one edge (to form a sinusoidal dipole) and the current at the other edge is set equal to zero. For this reason, the contributions from the line charges are omitted in the field expressions.

Fig. 2 illustrates a surface dipole in the yz plane with terminals at $z = 0$ and one ampere terminal current. At 300 MHz, the electric field intensity of this dipole (in free space) is listed in Table I.

REFERENCES

[1] S. A. Schelkunoff and H. T. Friis, *Antennas Theory and Practice*. New York: Wiley, 1952, pp. 370, 401.

[2] J. H. Richmond, "Computer program for thin-wire structures in a homogeneous conducting medium," National Technical Information Service, Springfield, VA 22161, Report NASA CR-2399, June 1974.

[3] ——, "Radiation and scattering by thin-wire structures in a homogeneous conducting medium," *IEEE Trans. Antennas Propagat.*, vol. AP-22, no. 2, p. 365, Mar. 1974.

[4] Y. T. Lin and J. H. Richmond, "EM modeling of aircraft at low frequencies," *IEEE Trans. Antennas Propagat.*, vol. AP-23, no. 1, pp. 53–56, Jan. 1975.

[5] N. N. Wang, J. H. Richmond, and M. C. Gilreath, "Sinusoidal reaction formulation for radiation and scattering from conducting surfaces," *IEEE Trans. Antennas Propagat.*, vol. AP-23, no. 3, pp. 376–382, May 1975.

APPENDIX B

Electromagnetic Modeling of Composite Wire and Surface Geometries

E. H. NEWMAN, MEMBER, IEEE, AND D. M. POZAR, STUDENT MEMBER, IEEE

Abstract—A moment method solution to the problem of radiation or scattering from geometries consisting of open or closed surfaces, wires, and wire/surface junctions is presented. The method is based on the sinusoidal reaction formulation. Several examples of input impedance calculations illustrate the versatility, accuracy, and computational efficiency of the method.

I. INTRODUCTION

THE METHOD of moments is perhaps the most widely used tool for the electromagnetic modeling of bodies which are not large in terms of a wavelength. The advantages of moment methods are accuracy, versatility, and the ability to compute near- as well as far-zone parameters.

The most widely used forms of the method of moments are the thin-wire computer programs [1]–[3]. These programs are ideal for modeling most wire antennas. By forming a wire-grid model they also can be used to model solid surfaces. Unfortunately, the size of the surface which can be modeled practically is severely limited since it requires many wires to accurately model a solid surface. Further, even a very fine wire mesh may not yield accurate near-zone parameters, such as current distribution or impedance.

More recently, surface-patch models have been developed for modeling solid surfaces. The advantage of the surface patch solution is that fewer unknowns are required per square wavelength of surface area. Wang *et al.* [4] have developed a model for wires and plates based on the sinusoidal reaction formulation. Albertsen *et al.* [5] used pulse expansion modes to model wires and plates, including the case where a wire touches a plate. Burke and Poggio have incorporated these results into a user-oriented computer code [3]. Parhami *et al.* have treated the problem of a wire surface junction using the finite difference technique [6].

The purpose of this paper is to present a technique for modeling wires and surfaces, including the case where the wires contact the surfaces, which is sufficiently accurate to compute impedance. The technique is based on the sinusoidal reaction formulation and is applicable to open as well as closed surfaces. Continuity of current is enforced on the wires, on the surfaces and at the wire/surface junctions. The accuracy and versatility of the model is demonstrated by several numerical examples. Attachment points are restricted to be somewhat removed from an edge.

II. THEORY

The Reaction Method

Consider a geometry of arbitrarily shaped scatterers in a homogeneous medium as shown in Fig. 1. S is the surface

Manuscript received October 14, 1977; revised February 23, 1978. This work was supported in part by the U.S. Army Research Office and in part by the Ohio State University Research Foundation, under Grant DAAG29-76-G-0331.

The authors are with the ElectroScience Laboratory, Department of Electrical Engineering, the Ohio State University, Columbus, OH 43212.

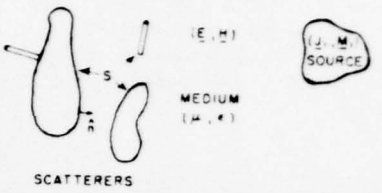

Fig. 1. General problem geometry.

enclosing the scatterers, and $\hat{n}$ is the unit outward normal to S. The scatterers may consist of solid surfaces and thin wires, and the wires may contact the surfaces. For now, the surfaces will be considered closed. The sources $(\mathbf{J}_i, \mathbf{M}_i)$ generate the fields $(\mathbf{E}, \mathbf{H})$ in the presence of the scatterers. The $e^{j\omega t}$ time dependence is suppressed. From the surface-equivalence theorem the field interior to the surface S will vanish without changing the exterior fields if the surface current densities

$$\mathbf{J}_s = \hat{n} \times \mathbf{H}, \tag{1}$$

$$\mathbf{M}_s = \mathbf{E} \times \hat{n} \tag{2}$$

are introduced on the surface S. The scattering obstacles may then be replaced by the ambient medium without altering the field anywhere. The scattered field, radiated by $(\mathbf{J}_s, \mathbf{M}_s)$ in the ambient medium, is defined as

$$\mathbf{E}_s = \mathbf{E} - \mathbf{E}_i \tag{3}$$

$$\mathbf{H}_s = \mathbf{H} - \mathbf{H}_i. \tag{4}$$

An electric test source, which radiates the fields $(\mathbf{E}_T, \mathbf{H}_T)$ in the ambient medium, is now placed in the interior region of S. Noting that this test source has zero reaction with the sources $(\mathbf{J}_s, \mathbf{M}_s)$ and $(\mathbf{J}_i, \mathbf{M}_i)$, the reaction integral equation [4] is obtained:

$$\iint_S (\mathbf{J}_s \cdot \mathbf{E}_T - \mathbf{M}_s \cdot \mathbf{H}_T)\, ds + \iiint_V (\mathbf{J}_i \cdot \mathbf{E}_T - \mathbf{M}_i \cdot \mathbf{H}_T)\, dv = 0 \tag{5}$$

where the volume integral is over the source volume. The reaction equation (5) is used to determine the unknown surface currents $(\mathbf{J}_s, \mathbf{M}_s)$. For conductors of finite conductivity the impedance boundary condition

$$\mathbf{M}_s = Z_s \mathbf{J}_s \times \hat{n} \tag{6}$$

is used where Z_s may be a function of position. For simplicity, only perfect conductors are considered here, thus $Z_s = \mathbf{M}_s = 0$.

In deriving (5) it was assumed that all surfaces were closed so that Schelkunoff's equivalence theorem could be used. However, it can be shown that (5) applies equally well for open surfaces. An open surface, such as a fictitious plate of

zero thickness, can be considered to be a limiting case of a real plate of finite thicknes as the plate thickness goes to zero. In general, different currents exist on the top and bottom surfaces of the real plate. As the plate thickness goes to zero, the fields radiated by the top and bottom currents become identical to the fields radiated by a single surface current located on the plate center. This single surface current is the vector sum of the top and bottom surface currents and is the current which must be determined to treat open surfaces. If electric test sources are used in (5), then $\mathbf{J}_s$ will be the vector sum of the current on the top and bottom surfaces [7].

The integral equation (5) is solved by the moment method. The unknown current $\mathbf{J}_s$ is expanded in a set of N basis (expansion) functions,

$$\mathbf{J}_s = \sum_{n=1}^{N} I_n \mathbf{J}_n, \tag{7}$$

and (5) is enforced for N electric test sources placed in S. Thus (5) reduces to the set of simultaneous linear equations

$$\sum_{n=1}^{N} I_n Z_{mn} = V_m; \qquad m = 1, 2 \cdots N \tag{8}$$

where

$$Z_{mn} = -\iint_n \mathbf{J}_n \cdot \mathbf{E}_m \, ds \tag{9}$$

$$V_m = \iiint_V (\mathbf{J}_i \cdot \mathbf{E}_m - \mathbf{M}_i \cdot \mathbf{H}_m) \, dv \tag{10}$$

where $(\mathbf{E}_m, \mathbf{H}_m)$ are the fields of the mth test source radiating in the medium (μ, ϵ) and the integration in (9) is over the surface of the nth expansion mode.

The expansion and test modes used here are identical. Thus the method is a Galerkin method, and a symmetric impedance matrix $[Z]$ results. The form of the expansion/test functions will now be defined. It is this form which ultimately determines the accuracy and efficiency of the solution as well as the types of geometries which may be modeled.

Expansion/Testing Functions

Three basic types of modes are used: wire dipole modes, surface dipole modes, and a special attachment mode whenever a wire connects to a surface. With this choice of functions geometries consisting of flat surfaces, thin wires, and wire-surface connections may be modeled. A piecewise flat approximation can be made to model singly curved surfaces. Note that all of the modes will involve sinusoids with the free-space wavenumber. This allows all but one of the integrations required to find the $\mathbf{E}_m$ to be done in closed form, thus avoiding the very difficult $1/r^3$ singularity or second derivative associated with finding the extreme near-zone fields of an electric current source, as is required to evaluate self or overlapping impedance elements Z_{mn}. The one integration not available in closed form is associated with the disk component of the attachment mode, as discussed below.

1) Thin-Wire Mode: The wire mode used is identical to that used by Richmond [1]. It is a piecewise-sinusoidal V-dipole consisting of two sinusoidal monopoles. A V-dipole with a 180° internal angle lying on the z-axis is shown in Fig. 2(a).

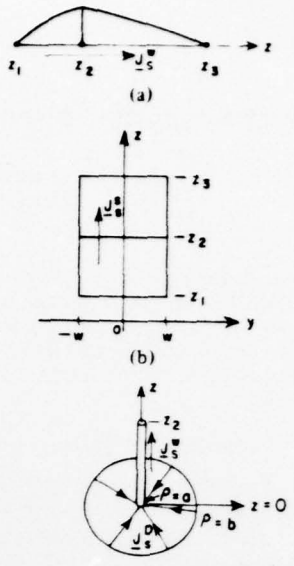

Fig. 2. Expansion and test modes. (a) Thin-wire V-dipole. (b) Sinusoidal surface V-dipole. (c) Attachment dipole.

Using the thin-wire approximation the current on this dipole is given by

$$\mathbf{J}_s^w = \frac{\hat{z}}{2\pi a}\left[P_1 \frac{\sin k(z - z_1)}{\sin k(z_2 - z_1)} + P_2 \frac{\sin k(z_3 - z)}{\sin k(z_3 - z_2)}\right] \tag{11}$$

where P_1 and P_2 represent pulse functions with unit value when $z_1 < z < z_2$ and $z_2 < z < z_3$, respectively, and are zero elsewhere. Also, a is the wire radius and $k = 2\pi/\lambda$. This choice of mode has the advantages that the near-zone fields and the Z_{mn} are known in closed form [8]. These modes are placed in an overlapping array on the wire ensuring continuity of current on the wire.

2) Surface-Patch Mode: The surface-patch mode is a surface V-dipole consisting of two sinusoidal surface monopoles. A surface V-dipole with interior angle of 180° is shown in Fig. 2(b). The current on this dipole is given by

$$\mathbf{J}_s^s = \hat{z}\frac{kP_1 \sin k(z - z_1)\cos ky}{2 \sin k(z_2 - z_1) \sin kw} + \hat{z}\frac{kP_2 \sin k(z_3 - z)\cos ky}{2 \sin k(z_3 - z_2) \sin kw} \tag{12}$$

where P_1 and P_2 represent unit pulse functions as before. This mode is similar to that used by Wang *et al.* [4] except that the sinusoidal variation is with the speed of light and a cosine variation is used transverse to $\mathbf{J}_s^s$ instead of the constant variation used by Wang *et al.* Because of this the fields due to the current of (12) may be found in closed form [9]. Two orthogonal and overlapping arrays of the surface-patch modes are placed on the surface, allowing a two-dimensional vector surface current density. Results presented in the next section indicate that reasonable accuracy can be obtained with $2w$ or $z_2 - z_2$ or $z_3 - z_2$ as large as 0.25 λ.

3) Attachment Mode: When a wire is attached to a surface a special attachment mode is introduced. The purpose of the attachment mode is twofold: first is to establish continuity of current at the wire/surface junction and second is to insure

that in the immediate vicinity of the attachment the surface current density has the proper $\hat{\rho}$ polarization and $1/\rho$ dependence. This mode consists of two parts: a wire monopole and a disk monopole, as shown in Fig. 2(c). The wire monopole current density is similar to the thin-wire monopole mode:

$$\mathbf{J}_s^w = \frac{I}{2\pi a} \frac{\sin k(z_2 - z)}{\sin kz_2} \hat{z}. \tag{13}$$

Thus

$$\mathbf{J}_s^D = \frac{-\sin k(b - \rho)}{2\pi\rho \sin k(b - a)} \hat{\rho}, \qquad a \leqslant \rho \leqslant b \tag{14}$$

where a, b are the inner and outer radii of the annulus. Note that the total current on the disk at $\rho = a$ is equal to the total current on the wire segment at $z = 0$ insuring continuity of current at the attachment. Also observe that the $\sin k(b - \rho)$ function in the numerator of (14) forces the disk current to be zero at the disk edge, $\rho = b$. It is this property which allows the disk to be placed on the surface and still maintain continuity of current on the surface. The $\sin k(b - \rho)$ function was chosen (rather than, say, $b - \rho$ or $\sin \alpha(b - \rho)$) since this permits the fields of the disk to be obtained with only one numerical integration.

The attachment mode is applied by placing it directly on the surface-patch modes wherever the wire meets the surface. Attachment points are not restricted to be in the center of or at the corners of the surface patch modes. However, a more detailed treatment of the attachment mode, including the edge singularity, would be required for attachment points less than about 0.1 λ from an edge. The inner radius a of the annulus corresponds to the wire radius, and results presented below indicate that the outer radius b has little effect on the final result if it is chosen to be between 0.1 λ to 0.25 λ (see Fig. 3).

With these expansion functions, current continuity in the direction of $\mathbf{J}_s$ is always maintained, although the current may not be continuous in directions orthogonal to the direction of current flow. Thus $\nabla \cdot \mathbf{J}_s = -j\omega\rho_s$ is always finite, and no line charges appear on the surface.

For antennas, feeds may be placed at the endpoints of any wire segment, including the attachment segment. For example, a monopole-on a ground plane may be modeled by inserting a generator at the base of the monopole between the attachment mode wire segment and disk. In the work presented here the delta-gap feed was used, although the magnetic frill model also could be used.

The scatterer or antenna geometry is thus modeled by N_w wire modes, N_s surface-patch modes, and N_A attachment modes. Then, $N = N_w + N_s + N_A$, and (8) is solved for the unknown current samples I_n by standard Gauss-Jordan elimination.

III. NUMERICAL EXAMPLES

Several numerical examples will now be presented which illustrate the accuracy and versatility of the solution presented in Section II. In each case, the number of modes used is summarized in Table I. Note that N_s is the total number of surface-patch dipoles. Thus there are $N_s/2$ dipoles in each of the two orthogonal directions on the surface. The data presented are input impedance or admittance, since this tends to be a sensitive indicator of overall accuracy.

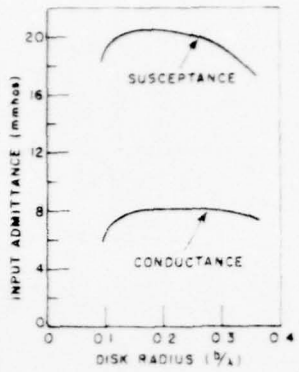

Fig. 3. Input admittance for geometry of Fig. 4, with $N = 14$, versus disk radius. $f = 160$ MHz.

TABLE I
PARAMETERS OF CALCULATIONS

FIGURE/CURVE	N_w	N_S	N_A	N(TOTAL UNKNOWNS)
3/ ——	2	12	1	15
4/ – – –	2	40	1	43
4/ ——	1	12	1	14
4/ — · —	121	-	-	121
5/ •••••	2	84	1	87
6/ •••••	2	21	1	24
7/ ——	4	12	1	17
8/ ——	4	12	2	18
9/ ——	7	77	3	87

In the experimental models the wires were brass rods, 0.0008 m in radius, with a conductivity of 15×10^6 mho/m. The finite conductivity of the wires was taken into account in the manner used by Richmond [10]. The metal plates were made of brass or aluminum, and their finite conductivity was not taken into account. In all cases the driven wire element was driven with a coaxial feed with outer radius 0.0047 m. All measurements were made by the authors.

The calculated results were all made using the same general purpose computer code. No advantage of inherent symmetries in the geometries was made. The resulting symmetries in the expansion mode currents offered a useful check on the calculations.

Fig. 4 presents the input admittance for a monopole on a square finite ground plane versus frequency in the vicinity of the first resonance. The calculation was done with $N = 14$ and with 43 unknowns and is compared with measured data and with a wire-grid model which used 121 unknowns. This example shows the accuracy and rapid convergence of the patch solution as well as a savings in storage over the wire-grid model. The run time for the $N = 14$ case was about 25 min on a Datacraft 6024/3, which is equivalent to about 2-3 min on an IBM 370-165.[1] In comparison the wire-grid model took about 40 min on the Datacraft 6024/3.

Fig. 3 shows the effect of the attachment disk radius b on the input admittance of the same geometry as Fig. 4. This graph shows that the disk radius is not critical and usually can be selected between 0.1 $\lambda \rightarrow$ 0.25 λ.

The impedance versus height of a monopole on a 1.4 λ square ground plane is shown in Fig. 5. These calculations are compared with the input impedance of a monopole of the same height on an infinite ground plane computed by image

[1] Recent improvements in the technique and computer code have reduced the run time by about a factor of 6, while increasing accuracy.

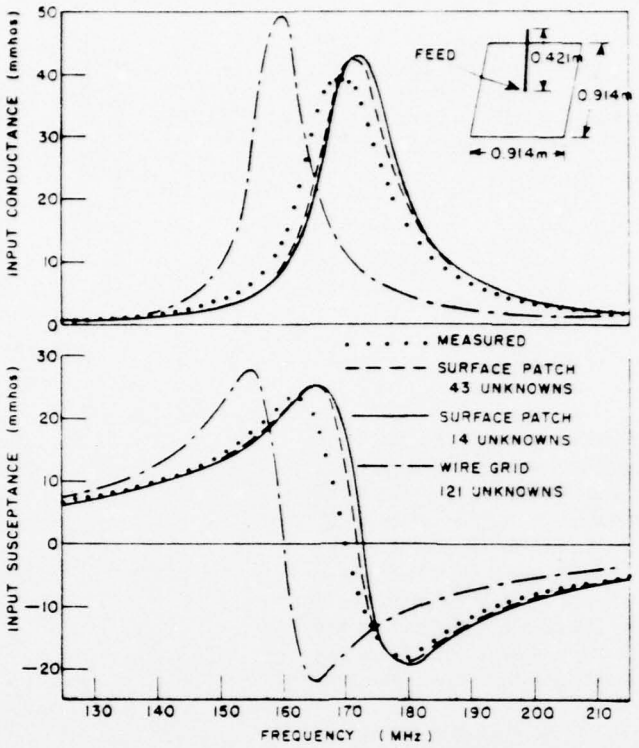

Fig. 4. Input admittance versus frequency for monopole (h = 0.421 m, a = 0.0008 m) on square ground plane (9.914 × 0.914 m), compared with measured data and wire-grid modeling. b = 0.2 λ.

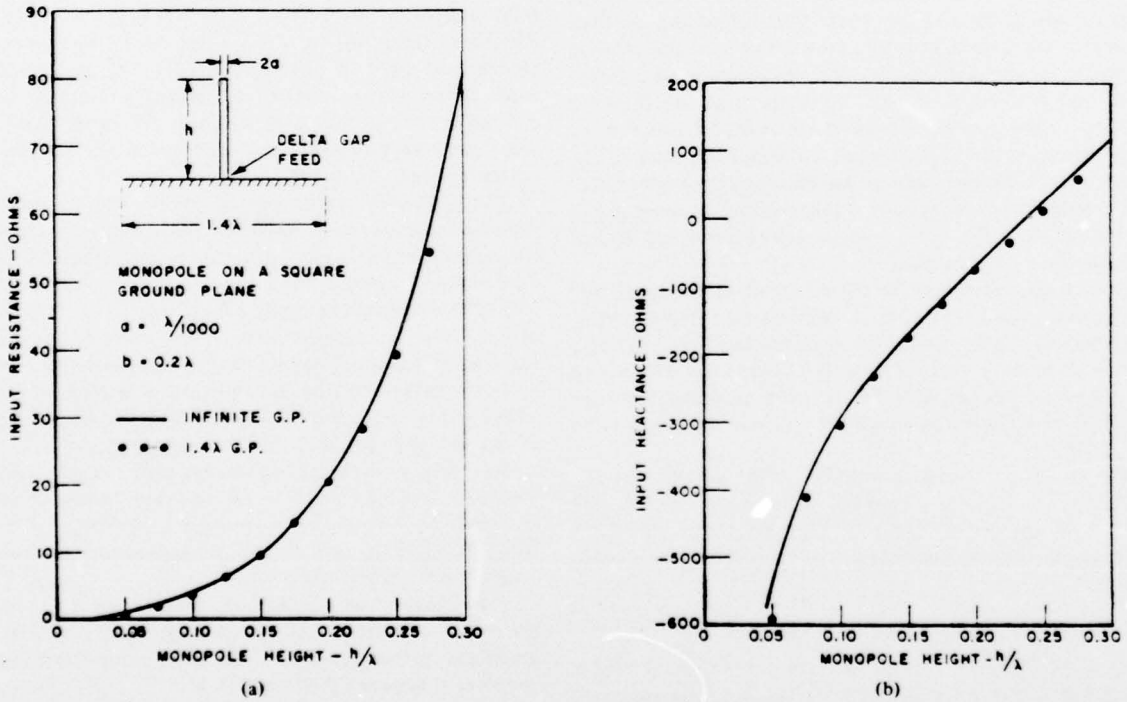

Fig. 5. (a) Input resistance versus monopole height for monopole centered on 1.4 λ square ground plane compared with same monopole on infinite ground plane as computed by image theory. (b) Input reactance versus monopole height for monopole centered on 1.4 λ square gound plane compared with same monopole on infinite ground plane, as computed by image theory.

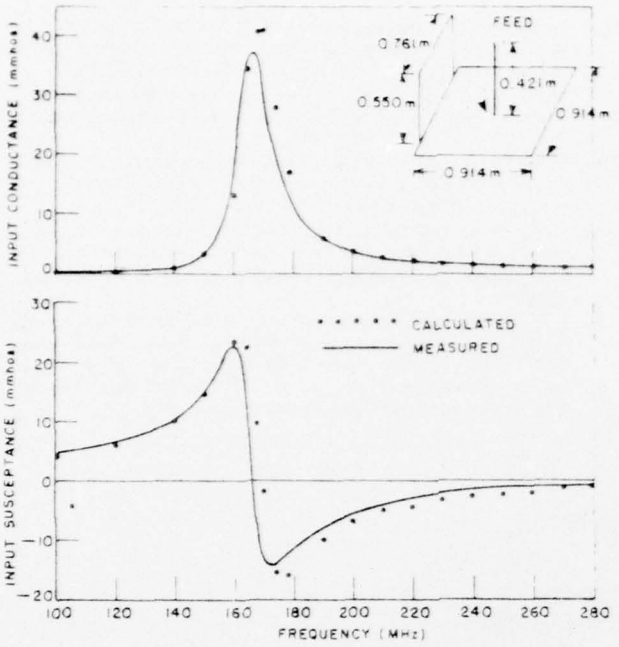

Fig. 6. Input admittance versus frequency for geometry of Fig. 4 with attached reflected plate compared with measured values.

theory. Since the 1.4 λ ground plane is fairly large, good agreement is obtained.

Fig. 6 shows the input admittance for a geometry identical to that of Fig. 3, except that a reflecting plate is attached to one side of the ground plane. Note that the width of the reflecting plate differs from that of the ground plane and that the theory and measurements are in close agreement. Overlap or hinge surface-patch dipoles are used to insure continuity of current at the plate to plate junction.

Fig. 7 shows the input admittance of the geometry of Fig. 3 with the addition of a parasitic wire element 1.5 cm above the ground plane and parallel to the fed monopole. The admittance is shown as a function of the separation d of the two wires. Fig. 8 shows a similar geometry except that the parasitic element now touches the ground plane.

Fig. 9 shows the measured and calculated input impedance of a T-bar fed, rectangular cavity-backed slot antenna opening into a finite ground plane.

IV. CONCLUSION

A moment method solution to the problem of radiation or scattering from geometries consisting of wires, open or closed surfaces, and wire surface junctions has been presented. The technique is a Galerkin solution based on the sinusoidal reaction formulation. The expansion and test modes were chosen to obtain continuity of current on the composite structure, the proper $\hat{\rho}/\rho$ behavior of the surface current density at attachment points, and facilitate the numerical evaluation of the impedance matrix. Numerical examples presented illustrate the accuracy, versatility, stability, and computational efficiency of the method. Future work will center on further improving the speed and computational efficiency of the method and adding the presence of dielectrics.

ACKNOWLEDGMENT

The authors wish to acknowledge the assistance of J. H. Richmond for helpful discussions and computer subroutines.

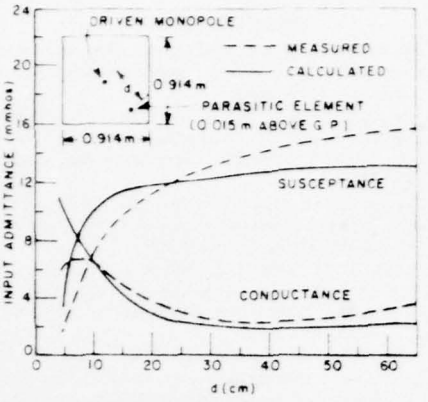

Fig. 7. Input admittance versus separation of driven monopole and parasitic wire element 0.015 m above the 0.0914 × 0.914 m ground plane. Driven monopole height = 0.421 m. Parasitic wire length = 0.842 m. f = 150 MHz.

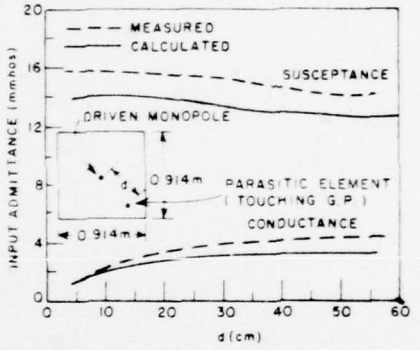

Fig. 8. Input admittance versus separation of driven monopole and parasitic wire element touching 0.914 × 0.914 m ground plane. Driven monopole height = 0.421 m. Parasitic wire height = 0.842 m. f = 150 MHz.

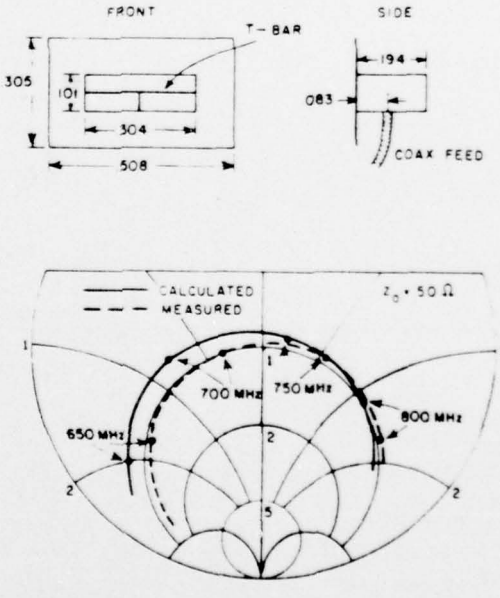

Fig. 9. Geometry and input impedance of T-bar fed slot antenna. Note: dimensions in meters.

REFERENCES

[1] J. H. Richmond, "A wire-grid model for scattering by conducting bodies," *IEEE Trans. Antennas Propagat.*, vol. AP-14, pp. 782–786, Nov. 1966.

[2] H. H. Chao and B. S. Strait, "Computer programs for radiation and scattering by arbitrary configurations of bent wires," Scientific Rep. 7 AFCRL-70-0374, Syracuse Univ., Syracuse, NY, Sept. 1970.

[3] G. J. Burke and A. J. Poggio, "Numerical electromagnetic code Method of moments," Naval Ocean Systems Center tech. document 116, AFWL-TR-76-320, July 1977.

[4] N. N. Wang, J. H. Richmond, and M. C. Gilreath, "Sinusoidal reaction formulation for radiation and scattering from conducting surfaces," *IEEE Trans. Antennas and Propagat.*, vol. AP-23, pp. 376–382, May 1975.

[5] N. C. Albertsen, J. E. Hansen, and N. E. Jensen, "Computation of radiation from wire antennas on conducting bodies," *IEEE Trans. Antennas and Propagat.*, vol. AP-22, pp. 200–206, Mar. 1974.

[6] P. Parhami, Y. Rahmat-Samii, and R. Mittra, "Investigation of antennas on a finite ground plane," *AP-S Int. Symp.*, Univ. of Massachusetts Amherst, Oct. 11–15, 1976, pp. 511–514.

[7] W. A. Davis and R. Mittra, "A new approach to the thin scatterer problem using the hybrid equations," *IEEE Trans. Antennas and Propagat.*, vol. AP-25, May 1977.

[8] J. H. Richmond and N. H. Geary, "Mutual impedance of nonplanar-skew sinusoidal dipoles," *IEEE Trans. Antennas and Propagat.*, vol. AP-23, May 1975.

[9] J. H. Richmond, D. M. Pozar, and E. H. Newman, "Rigorous near-zone field expressions for rectangular sinusoidal monopole," *IEEE Trans. Antennas and Propagat.*, vol. AP-26, p. 509, May 1978.

[10] J. H. Richmond, "Radiation and scattering by thin-wire structures in the complex frequency domain," Rep. 2902-10, Ohio State Univ. ElectroScience Laboratory, Dep. of Electrical Engineering, prepared under Grant NGL 35-008-138 for National Aeronautics and Space Administration, July 1973.

APPENDIX C

Near fields of a vector electric line source near the edge of a wedge

D. M. Pozar and E. H. Newman

ElectroScience Laboratory, Department of Electrical Engineering, Ohio State University, Columbus, Ohio 43212

(Received July 19, 1978.)

Simple closed form expressions are obtained for the fields of an electric line source with transverse or longitudinal current flow parallel to and near the edge of a perfectly conducting wedge. The effect of an edge which is not perfectly sharp is investigated by considering a cylinder-tipped half plane.

1. INTRODUCTION

The problem of scattering by wedges has been treated extensively by many authors [*Bowman et al.*, 1969; *Felsen and Marcuvitz*, 1973]. Usually the analysis involves asymptotic methods for evaluating far fields, with little emphasis on near-field calculations. It is the near-field aspect with which the present paper is concerned.

An interest in the near zone fields of a source near an edge arises when formulating a moment method solution to the problem of a wire antenna mounted near the edge of a plate or wedge. In a previous paper [*Newman and Pozar*, 1978] the authors presented a moment method technique whereby problems with wires mounted 0.1λ or greater from an edge may be treated. The analysis presented here forms a first step in extending this technique by synthesizing an expansion mode to treat the case of the wire near an edge. A wire attached near the edge of a wedge may have current transverse or parallel to the edge. Thus a vector electric line source parallel to the edge but with current transverse or parallel to the edge is considered. Simple expressions for the near zone fields are derived which exhibit not only the correct edge behavior but the source singularity as well.

2. THEORY FOR PERFECTLY CONDUCTING WEDGE

A. *Introduction.* The geometry of the problem is shown in Figure 1. The field point is (ρ, ϕ) while the electric line source is at (ρ', ϕ'), $0 \leq \phi, \phi' \leq 2\pi - \phi_0$. The line source is parallel to the edge of the wedge and has components I_ρ, I_ϕ, and I_z of current in the $\hat{\rho}$, $\hat{\phi}$, and $\hat{z}$ directions, respectively. The current is assumed to be constant with respect to z. Thus the source current density may be written as

$$\mathbf{J}(\rho, \phi) = (I_\rho \hat{\rho} + I_\phi \hat{\phi} + I_z \hat{z}) \frac{1}{\rho} \delta(\rho - \rho') \cdot \delta(\phi - \phi') A / M^2 \qquad (1)$$

The method of solution is to use the two-dimensional dyadic Green's function for the wedge to find the magnetic field due to the vector current $\mathbf{J}$. Then, since the field and source points are close to the edge, small argument approximations are used for the Bessel functions which occur in the resulting infinite series. The series is then summed in closed form, preserving the source singularity. Maxwell's equations are used to find the $\mathbf{E}$ fields. Of course, with the fields of an electric source known the fields of a magnetic source may be found from duality.

B. *Two-dimensional dyadic Green's function.* The two-dimensional dyadic Green's function is a solution of the vector wave equation [*Tai*, 1973]

$$(\nabla \times \nabla \times - k^2)\bar{\mathbf{G}}_{m2}(\mathbf{R}|\mathbf{R}') = \nabla \times [\bar{\mathbf{I}}\delta(\mathbf{R} - \mathbf{R}')] \qquad (2)$$

where $k = 2\pi/\lambda_0$, $\bar{\mathbf{I}}$ is the unit dyad, $\mathbf{R} = \rho\hat{\rho} + \phi\hat{\phi}$, $\mathbf{R}' = \rho'\hat{\rho} + \phi'\hat{\phi}$, and $\bar{\mathbf{G}}_{m2}$ satisfies the boundary condition $\hat{n} \times \nabla \times \bar{\mathbf{G}}_{m2} = 0$ on S. The fields are then found from

$$\mathbf{H}(\mathbf{R}) = \int \bar{\mathbf{G}}_{m2}(\mathbf{R}|\mathbf{R}') \cdot \mathbf{J}(\mathbf{R}')\, ds \qquad (3)$$

and, assuming $e^{j\omega t}$ time dependence,

$$\mathbf{E}(\mathbf{R}) = \frac{1}{j\omega\varepsilon_0} [\nabla \times \mathbf{H}(\mathbf{R}) - \mathbf{J}(\mathbf{R})] \qquad (4)$$

The integration in (3) is over the source region.

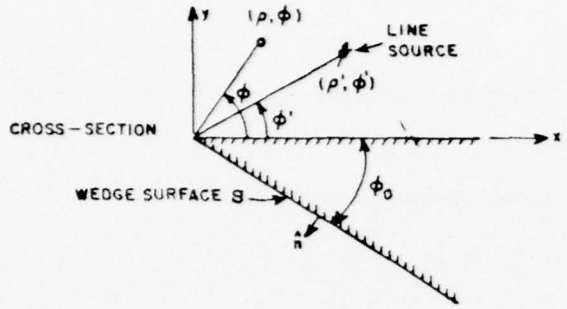

Fig. 1. Geometry of the line source near an edge.

Using (1) in (3) gives

$$\mathbf{H}(\mathbf{R}) = I_\rho \bar{\mathbf{G}}_{m2}(\mathbf{R}|\mathbf{R}') \cdot \hat{\rho} + I_\phi \bar{\mathbf{G}}_{m2}(\mathbf{R}|\mathbf{R}') \cdot \hat{\phi} + I_z \bar{\mathbf{G}}_{m2}(\mathbf{R}|\mathbf{R}') \cdot \hat{z} \quad (5)$$

The Green's function $\bar{\mathbf{G}}_{m2}$ is given by *Tai* [1971, 1973] (note that from (1), $\nabla \cdot \bar{\mathbf{G}}_{m2} = 0$, so that only the **M** and **N** vector wave functions are needed in the eigenfunction expansion of $\bar{\mathbf{G}}_{m2}$):

$$\bar{\mathbf{G}}_{m2}(\mathbf{R}|\mathbf{R}') = \frac{2}{(2\pi - \phi_0)} \int_0^\infty d\lambda \sum_{n=0}^{\infty} \frac{\mathbf{M}_{o_{e}\alpha\lambda} \mathbf{N}'_{o_{e}\alpha\lambda} + \mathbf{N}_{o_{e}\alpha\lambda} \mathbf{M}'_{o_{e}\alpha\lambda}}{(1 + \delta_0)(\lambda^2 - k^2)} \quad (6)$$

where

$$\delta_0 = \begin{cases} 1 & n = 0 \\ 0 & n \neq 0 \end{cases} \qquad \alpha = n\nu = n\frac{\pi}{(2\pi - \phi_0)}$$

$n = 0, 1, 2, \cdots$, and the vector wave functions are (the two-dimensional form of the vector wave functions given above is most easily found from the three-dimensional form given by [*Tai*, 1971] by letting $h = 0$)

$$\mathbf{M}_{o_{e}\alpha\lambda} = \mp \frac{\alpha}{\rho} J_\alpha(\lambda\rho) \begin{matrix}\sin \\ \cos\end{matrix} \alpha\phi\hat{\rho} - \lambda J'_\alpha(\lambda\rho) \begin{matrix}\cos \\ \sin\end{matrix} \alpha\phi\hat{\phi}$$
$$\mathbf{N}_{o_{e}\alpha\lambda} = J_\alpha(\lambda\rho) \begin{matrix}\cos \\ \sin\end{matrix} \alpha\phi\hat{z} \quad (7)$$

Consistent with *Tai*'s [1971] notation, **M**′ and **N**′ in (6) refer to **M** and **N** with primed spatial (source) coordinates, whereas elsewhere the prime refers to differentiation with respect to the argument.

In defining field components, superscripts refer to the source polarization and subscripts refer to the field component. Then, from (5)–(7), $H^\rho_\rho = H^\rho_\phi = H^\phi_\phi = H^\phi_\rho = H^z_z = 0$, and

$$H^\rho_z(\rho, \phi) = \frac{-2I_\rho}{(2\pi - \phi_0)\rho'} \int_0^\infty d\lambda \sum_{n=0}^{\infty} \frac{\alpha\lambda J_\alpha(\lambda\rho) J_\alpha(\lambda\rho')}{(1 + \delta_0)(\lambda^2 - k^2)} \cos\alpha\phi \sin\alpha\phi' \quad (8)$$

$$H^\phi_z(\rho, \phi) = \frac{-2I_\phi}{(2\pi - \phi_0)} \int_0^\infty d\lambda \sum_{n=0}^{\infty} \frac{\lambda^2 J_\alpha(\lambda\rho) J'_\alpha(\lambda\rho')}{(1 + \delta_0)(\lambda^2 - k^2)} \cos\alpha\phi \cos\alpha\phi' \quad (9)$$

$$H^z_\rho(\rho, \phi) = \frac{2I_z}{(2\pi - \phi_0)\rho} \int_0^\infty d\lambda \sum_{n=0}^{\infty} \frac{\alpha\lambda J_\alpha(\lambda\rho) J_\alpha(\lambda\rho')}{(1 + \delta_0)(\lambda^2 - k^2)} \cos\alpha\phi \sin\alpha\phi' \quad (10)$$

$$H^z_\phi(\rho, \phi) = \frac{-2I_z}{(2\pi - \phi_0)} \int_0^\infty d\lambda \sum_{n=0}^{\infty} \frac{\lambda^2 J'_\alpha(\lambda\rho) J_\alpha(\lambda\rho')}{(1 + \delta_0)(\lambda^2 - k^2)} \sin\alpha\phi \sin\alpha\phi' \quad (11)$$

The integrations in (8)–(11) can be evaluated [*Tai*, 1971] to give

$$H^\rho_z(\rho, \phi) = \frac{j\pi I_\rho}{(2\pi - \phi_0)\rho'} \sum_{n=0}^{\infty} \frac{\alpha \cos\alpha\phi \sin\alpha\phi'}{(1 + \delta_0)} \cdot \begin{cases} J_\alpha(k\rho) H^{(2)}_\alpha(k\rho') & \rho < \rho' \\ H^{(2)}_\alpha(k\rho) J_\alpha(k\rho') & \rho > \rho' \end{cases} \quad (12)$$

$$H^\phi_z(\rho, \phi) = \frac{j\pi k I_\phi}{(2\pi - \phi_0)} \sum_{n=0}^{\infty} \frac{\cos\alpha\phi \cos\alpha\phi'}{(1 + \delta_0)} \cdot \begin{cases} J_\alpha(k\rho) H^{(2)\prime}_\alpha(k\rho') & \rho < \rho' \\ H^{(2)}_\alpha(k\rho) J'_\alpha(k\rho') & \rho > \rho' \end{cases} \quad (13)$$

$$H^z_\rho(\rho, \phi) = \frac{-j\pi I_z}{(2\pi - \phi_0)\rho} \sum_{n=0}^{\infty} \frac{\alpha \cos\alpha\phi \sin\alpha\phi'}{(1 + \delta_0)} \cdot \begin{cases} J_\alpha(k\rho) H^{(2)}_\alpha(k\rho') & \rho < \rho' \\ H^{(2)}_\alpha(k\rho) J_\alpha(k\rho') & \rho > \rho' \end{cases} \quad (14)$$

$$H^z_\phi(\rho, \phi) = \frac{j\pi k I_z}{(2\pi - \phi_0)} \sum_{n=0}^{\infty} \frac{\sin\alpha\phi \sin\alpha\phi'}{(1 + \delta_0)} \cdot \begin{cases} J'_\alpha(k\rho) H^{(2)}_\alpha(k\rho') & \rho < \rho' \\ H^{(2)\prime}_\alpha(k\rho) J_\alpha(k\rho') & \rho > \rho' \end{cases} \quad (15)$$

Up to this point the field expressions are completely rigorous.

C. *Near-field calculation.* The source and field points are now restricted to be close to the edge of the wedge, so $k\rho < 1$ and $k\rho' < 1$. Using small argument approximations for the Bessel functions in (12)–(15) and trigonometric identities yields

$$H_z^w(\rho, \phi) = \frac{-I_w}{(2\pi - \phi_0)\rho'} \begin{cases} \frac{1}{2}\sum_{n=1}^{\infty}\left(\frac{\rho}{\rho'}\right)^{\alpha}[\sin\alpha(\phi+\phi') - \sin\alpha(\phi-\phi')] & \rho < \rho' \\ \frac{1}{2}\sum_{n=1}^{\infty}\left(\frac{\rho'}{\rho}\right)^{\alpha}[\sin\alpha(\phi+\phi') - \sin\alpha(\phi-\phi')] & \rho > \rho' \end{cases} \tag{16}$$

$$H_z^b(\rho, \phi) = \frac{I_b}{(2\pi - \phi_0)\rho'} \begin{cases} \frac{1}{2}\sum_{n=0}^{\infty}\left(\frac{\rho}{\rho'}\right)^{\alpha}[\cos\alpha(\phi+\phi') + \cos\alpha(\phi-\phi')] & \rho < \rho' \\ \frac{-1}{2}\sum_{n=0}^{\infty}\left(\frac{\rho'}{\rho}\right)^{\alpha}[\cos\alpha(\phi+\phi') + \cos\alpha(\phi-\phi')] + 1 & \rho > \rho' \end{cases} \tag{17}$$

$$H_\rho^z(\rho, \phi) = \frac{I_z}{(2\pi - \phi_0)\rho} \begin{cases} \frac{1}{2}\sum_{n=1}^{\infty}\left(\frac{\rho}{\rho'}\right)^{\alpha}[\sin\alpha(\phi+\phi') - \sin\alpha(\phi-\phi')] & \rho < \rho' \\ \frac{1}{2}\sum_{n=1}^{\infty}\left(\frac{\rho'}{\rho}\right)^{\alpha}[\sin\alpha(\phi+\phi') - \sin\alpha(\phi-\phi')] & \rho > \rho' \end{cases} \tag{18}$$

$$H_\phi^z(\rho, \phi) = \frac{I_z}{(2\pi - \phi_0)\rho} \begin{cases} \frac{1}{2}\sum_{n=1}^{\infty}\left(\frac{\rho}{\rho'}\right)^{\alpha}[\cos\alpha(\phi+\phi') - \cos\alpha(\phi-\phi')] & \rho < \rho' \\ \frac{-1}{2}\sum_{n=1}^{\infty}\left(\frac{\rho'}{\rho}\right)^{\alpha}[\cos\alpha(\phi+\phi') - \cos\alpha(\phi-\phi')] & \rho > \rho' \end{cases} \tag{19}$$

Using the summation formulas (A3) and (A4) given in the Appendix, after simplification, the desired closed form results:

$$H_z^w(\rho, \phi) = \frac{-I_w\rho^{\nu}\rho'^{\nu-1}}{2(2\pi - \phi_0)} \cdot \left[\frac{\sin\nu(\phi+\phi')}{R_+} - \frac{\sin\nu(\phi-\phi')}{R_-}\right] \tag{20}$$

$$H_z^b(\rho, \phi) = \frac{I_b\rho'^{\nu-1}}{2(2\pi - \phi_0)} \cdot \left[\frac{\rho'^{\nu} - \rho^{\nu}\cos\nu(\phi+\phi')}{R_+} + \frac{\rho'^{\nu} - \rho^{\nu}\cos\nu(\phi-\phi')}{R_-}\right] \tag{21}$$

$$H_\rho^z(\rho, \phi) = \frac{I_z\rho^{\nu-1}\rho'^{\nu}}{2(2\pi - \phi_0)} \cdot \left[\frac{\sin\nu(\phi+\phi')}{R_+} - \frac{\sin\nu(\phi-\phi')}{R_-}\right] \tag{22}$$

$$H_\phi^z(\rho, \phi) = \frac{I_z\rho^{\nu-1}}{2(2\pi - \phi_0)} \cdot \left[\frac{\rho'^{\nu}\cos\nu(\phi+\phi') - \rho^{\nu}}{R_+} - \frac{\rho'^{\nu}\cos\nu(\phi-\phi') - \rho^{\nu}}{R_-}\right] \tag{23}$$

where $\nu = \pi/(2\pi - \phi_0)$ and

$$R_\pm = \rho^{2\nu} + \rho'^{2\nu} - 2\rho^{\nu}\rho'^{\nu}\cos\nu(\phi \pm \phi')$$

The **E** fields could be found either by using (4) on (12)–(15) and applying the procedure of small argument approximations and summation of the series or by using (4) on (20)–(23) directly. Identical results are obtained with either method for all **E** components except for E_z^z, which would reduce to zero if the curl of (22), (23) were taken. Thus E_z^z is found from (4) and (14)–(15), while the other **E** components are found by using (4) and (20), (21). After simplification, $E_z^\phi = E_z^w = E_w^z = E_b^z = 0$, and

$$E_w^w(\rho, \phi) = \frac{I_w\nu(\rho\rho')^{\nu-1}}{2j\omega\varepsilon_0(2\pi - \phi_0)} \cdot \left[\frac{2\rho^{\nu}\rho'^{\nu} - (\rho^{2\nu} + \rho'^{2\nu})\cos\nu(\phi+\phi')}{R_+^2}\right.$$

$$- \frac{2\rho^{\nu}\rho'^{\nu} - (\rho^{2\nu} + \rho'^{2\nu})\cos\nu(\phi - \phi')}{R^2}\Bigg] - \frac{I_\rho}{j\omega\varepsilon_0\rho}\delta(\rho - \rho')\delta(\phi - \phi') \tag{24}$$

$$E^{\rho}_{\phi}(\rho, \phi) = \frac{I_\rho \nu(\rho\rho')^{\nu-1}}{2j\omega\varepsilon_0(2\pi - \phi_0)}\left[\frac{(\rho'^{2\nu} - \rho^{2\nu})\sin\nu(\phi + \phi')}{R_+^2} - \frac{(\rho'^{2\nu} - \rho^{2\nu})\sin\nu(\phi - \phi')}{R^2}\right] \tag{25}$$

$$E^{\phi}_{\rho}(\rho, \phi) = \frac{I_\phi \nu(\rho\rho')^{\nu-1}}{2j\omega\varepsilon_0(2\pi - \phi_0)}\left[\frac{(\rho^{2\nu} - \rho'^{2\nu})\sin\nu(\phi + \phi')}{R_+^2} + \frac{(\rho^{2\nu} - \rho'^{2\nu})\sin\nu(\phi - \phi')}{R^2}\right] \tag{26}$$

$$E^{\phi}_{\phi}(\rho, \phi) = \frac{I_\phi \nu(\rho\rho')^{\nu-1}}{2j\omega\varepsilon_0(2\pi - \phi_0)}\cdot\left[\frac{2\rho^{\nu}\rho'^{\nu} - (\rho'^{2\nu} + \rho^{2\nu})\cos\nu(\phi + \phi')}{R_+^2} + \frac{2\rho^{\nu}\rho'^{\nu} - (\rho'^{2\nu} + \rho^{2\nu})\cos\nu(\phi - \phi')}{R^2}\right] - \frac{I_\phi}{j\omega\varepsilon_0\rho}\delta(\rho - \rho')\delta(\phi - \phi') \tag{27}$$

From (4), (14), and (15),

$$E^{z}_{z}(\rho, \phi) = \frac{-\pi k^2 I_z}{\omega\varepsilon_0(2\pi - \phi_0)}\cdot\sum_{n=1}^{\infty}\sin\alpha\phi\sin\alpha\phi' J_\alpha(k\rho)H^{(2)}_\alpha(k\rho') - \frac{I_z}{j\omega\varepsilon_0\rho}\delta(\rho - \rho')\delta(\phi - \phi') \qquad \rho < \rho'$$

$$E^{z}_{z}(\rho, \phi) = \frac{-\pi k^2 I_z}{\omega\varepsilon_0(2\pi - \phi_0)}\cdot\sum_{n=1}^{\infty}\sin\alpha\phi\sin\alpha\phi' H^{(2)}_\alpha(k\rho)J_\alpha(k\rho') - \frac{I_z}{j\omega\varepsilon_0\rho}\delta(\rho - \rho')\delta(\phi - \phi') \qquad \rho > \rho' \tag{28}$$

Using small argument approximations in the Bessel functions in (28) gives

$$E^{z}_{z}(\rho, \phi) = \frac{jk^2 I_z}{2\pi\omega\varepsilon_0}\cdot\sum_{n=1}^{\infty}[\cos\alpha(\phi + \phi') - \cos\alpha(\phi - \phi')]\frac{1}{n}\left(\frac{\rho}{\rho'}\right)^{n} - \frac{I_z}{j\omega\varepsilon_0\rho}\delta(\rho - \rho')\delta(\phi - \phi') \qquad \rho < \rho'$$

$$E^{z}_{z}(\rho, \phi) = \frac{jk^2 I_z}{2\pi\omega\varepsilon_0}\cdot\sum_{n=1}^{\infty}[\cos\alpha(\phi + \phi') - \cos\alpha(\phi - \phi')]\frac{1}{n}\left(\frac{\rho'}{\rho}\right)^{n} - \frac{I_z}{j\omega\varepsilon_0\rho}\delta(\rho - \rho')\delta(\phi - \phi') \qquad \rho > \rho' \tag{29}$$

Using the summation formula (A7) of the Appendix gives

$$E^{z}_{z}(\rho, \phi) = \frac{-jk^2 I_z}{4\pi\omega\varepsilon_0}\ln\left[\frac{R_+}{R}\right] - \frac{I_z}{j\omega\varepsilon_0\rho}\delta(\rho - \rho')\delta(\phi - \phi') \tag{30}$$

Equations (20)–(23), (24)–(27), and (30) are the complete field expressions for an arbitrary vector electric line source and are rigorous in the near-field limit, including the proper source singularity. Note the proper edge behavior in the fields as $\rho \to 0$. Also note that the expressions for **H** in (20)–(23) are independent of frequency, indicating a quasi-static result. Hence (20)–(23) could have been obtained from a conformal mapping approach.

Figure 2 shows the magnitude of E^{ϕ}_{ϕ} versus distance along the surface of the wedge for various wedge angles and $\lambda = 1$ m, $\rho' = 0.1$ m, $\phi' = 0$, and $I_\phi = 1$.

Although the transverse field components are singular at the edge of the ideal wedge, no such singularity exists on any physically realizable electromagnetic scatterer. The reason for this difference is that the ideal wedge has a perfectly sharp edge with a discontinuous normal vector, while in physical reality any real 'edge' will have a small radius of curvature so that the normal vector at the 'edge' will change continuously as it moves around the 'edge.' This fact was recently used by *Rhodes* [1971] in connection with physically realizable antenna aperture distributions.

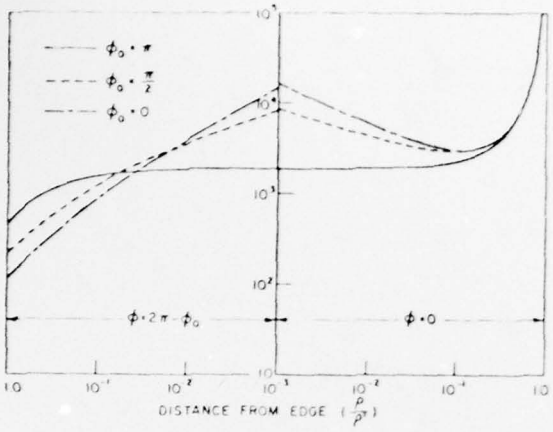

Fig. 2. Magnitude of E_ϕ^ϕ (phase = $-90°$) versus normalized distance along both sides of the wedge surface for various wedge angles, $\rho' = 0.1$ m, $\lambda = 1$ m, $\phi' = 0$, $I_\phi = 1$.

Another interesting observation is that some field components away from the edge become singular when the line source approaches the edge ($\rho' \to 0$). This is in agreement with reciprocity. Of course, this situation could never happen in practice because the perfectly sharp wedge does not exist.

In order to get a feeling for the field behavior at a physical 'edge' the mathematically ideal edge of the wedge of this section is removed by adding a circular cylinder tip. Although this geometry is not an exact model of a physical edge, it should allow a qualitative view of the field behavior, with the advantage that it is mathematically tractable.

3. THE CYLINDER-TIPPED HALF PLANE

By using the same method as that outlined in section 2, the closed form field equations for a cylinder-tipped wedge may be obtained. Here, only the expression for E_ϕ^ϕ for the special case of a half plane ($\phi_0 = 0$) with an I_ϕ line source ($I_z = I_\rho = 0$) on the surface of the half plane ($\phi' = 0$) is presented.

The geometry for the cylinder-tipped half plane is shown in Figure 3. The two-dimensional dyadic Green's function may be obtained from the three-dimensional result given by *Tai* [1971] as described in section 2. The Green's function is seen to consist of a sum of the half-plane Green's function and terms which account for scattering from the cylindrical tip. Thus

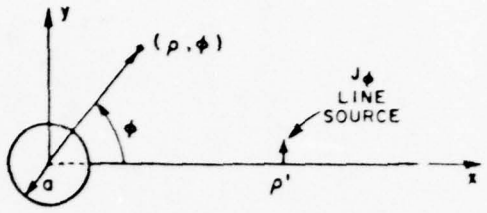

Fig. 3. Geometry of an electric line source on the surface and close to the edge of a cylinder-tipped half plane. Current polarization is in the ϕ (or $\hat{y}$) direction.

$$\mathbf{E}^\phi(\mathbf{R}) = \mathbf{E}^{\phi(\text{wedge})}(\mathbf{R}) + \mathbf{E}^{\phi(\text{cyl})}(\mathbf{R})$$

where $\bar{E}^{\phi(\text{wedge})}(\bar{R})$ is given by (26) and (27). Omitting the detailed derivation, for $k\rho < 1$ and $k\rho' < 1$,

$$E_\phi^{\phi(\text{cyl})}(\rho, \phi) = \frac{I_\phi}{4\pi j\omega\varepsilon_0\rho\rho'} \cdot \frac{[(a^2/\rho\rho')^{1/2} + (a^2/\rho\rho')^{3/2}]\cos\frac{\phi}{2} - 2(a^2/\rho\rho')}{\left[1 - 2(a^2/\rho\rho')^{1/2}\cos\frac{\phi}{2} + (a^2/\rho\rho')\right]^2} \tag{31}$$

The total E_ϕ^ϕ field for $y = 0$, $\phi' = 0$, $\phi_0 = 0$, $\rho' = 0.1$ m, $\lambda = 1$ m is plotted versus $\rho = x$ for various values of a for the cylinder-tipped half plane in Figure 4. Also shown in this figure is the E_ϕ^ϕ field for a perfectly sharp half plane, which would correspond to $a = 0$ (no cylinder tip). Figure 5 shows the same curves for $\rho' = 0.01$ ($\lambda = 1$ m). The $\rho = x$ axis is logarithmic to give an expanded view of the edge area. First of all, note that for $a = 0$ (no cylinder) the field is becoming singular as expected. Now, for a small but finite cylinder radius a the E_ϕ^ϕ field increases as the edge is approached but reaches a maximum and goes to zero at $\rho = a$, as is required by boundary conditions. It can be seen from Figures 4 and 5 that the field reaches a higher maximum for smaller a but is not singular except for $a = 0$.

Figure 6 shows the total E_ϕ^ϕ field for $y = 0$, $\phi' = 0$, $\phi_0 = 0$, $\rho' = 0.1$ m, $\lambda = 1$ m, and $a = 5 \times 10^{-4}$ m versus $\rho = x$ on a rectangular scale for the ideal half plane and the cylinder-tipped half plane, along with a sketch of the relative size of

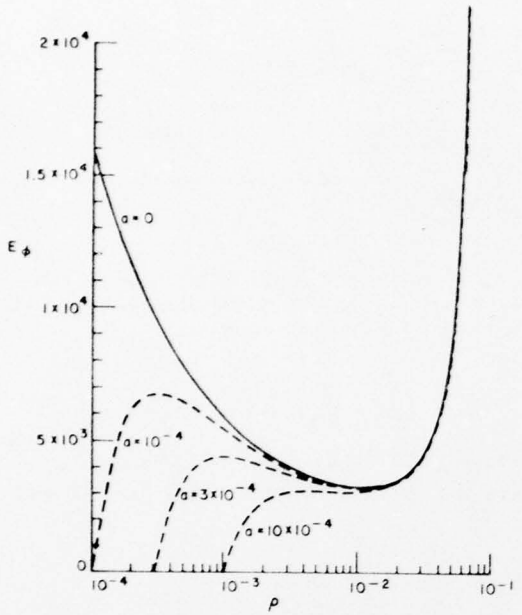

Fig. 4. Magnitude of E_ϕ^s (phase = $-90°$) versus position (ρ = x) along the surface of a cylinder-tipped half plane for various values of cylinder tip radius a, $\rho' = 0.1$ m, $\lambda = 1$ m, $\phi' = 0$, $\phi = 0$, $I_0 = 1$, $\phi_0 = 0$ (half plane).

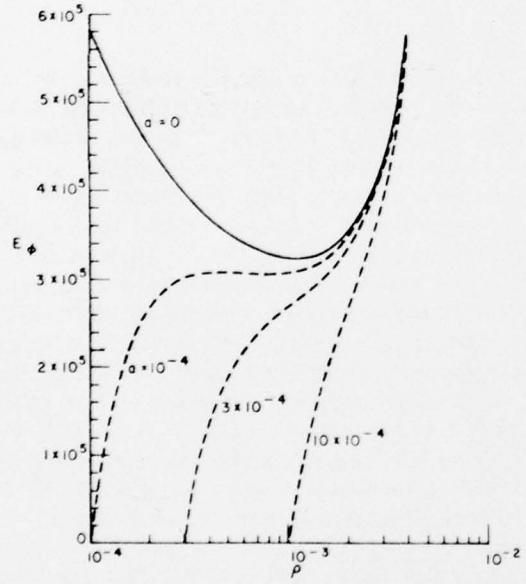

Fig. 5. Magnitude of E_ϕ^s (phase = $-90°$) versus position (ρ = x) along the surface of a cylinder-tipped half plane for various values of cylinder tip radius a, $\rho' = 0.01$ m, $\lambda = 1$ m, $\phi' = 0$, $\phi = 0$, $I_0 = 1$, $\phi_0 = 0$ (half plane).

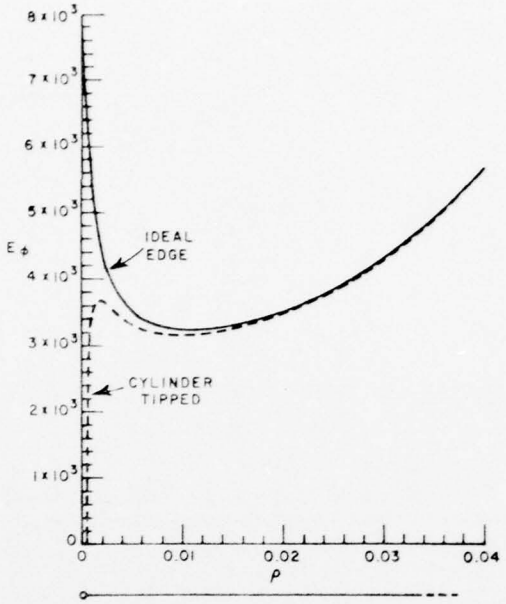

Fig. 6. Magnitude of E_ϕ^s (phase = $-90°$) versus position (ρ = x) along the surface of a cylinder-tipped half plane compared with that for an ideal half plane. The relative size of the cylindrical tip is also shown, $\rho' = 0.1$ m, $\lambda = 1$ m, $\phi' = 0$, $\phi = 0$, $I_0 = 1$, $a = \rho'/200$.

the cylinder. Figure 7 shows the same curves for $a = 5 \times 10^{-5}$ m.

4. CONCLUSION

Simple closed form expressions have been derived and presented for the fields of an electric line source with arbitrary current flow near and parallel to the edge of a perfectly conducting wedge. The effect of a physical edge (not perfectly sharp) has been investigated by comparing the fields near the end of a cylinder-tipped half plane with those near the edge of an ideal half plane.

The above results show that for even a small departure from an ideal edge the fields will not be singular. Since any physical scattering edge has a certain degree of roundness or roughness, singularities will not be found in the edge vicinity. It should be mentioned that there is not universal agreement on the interpretation of the differences between ideal edges and physical edges [*Lee*, 1972]. However, it is clear from the data presented that for a source in the near vicinity of an edge the

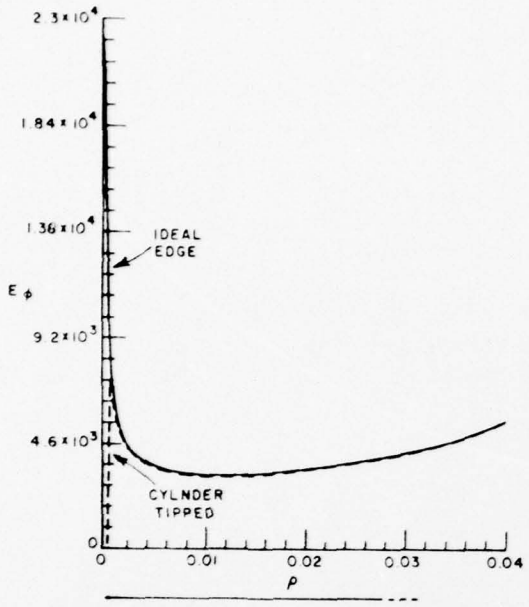

Fig. 7. Magnitude of E_ϕ^z (phase = −90°) versus position ($\rho = x$) along the surface of a cylinder-tipped half plane compared with that for an ideal half plane. The relative size of the cylindrical tip is also shown. $\rho' = 0.1$ m, $\lambda = 1$ m, $\phi' = 0$, $\phi = 0$, $I_\phi = 1$, $a = \rho'/2000$.

'edge' behavior of the fields is confirmed to a region a few thousandths of a wavelength from the edge.

APPENDIX: SUMMATION OF SERIES

Starting with the known result

$$\sum_{n=0}^{\infty} a^n x^n = \frac{1}{1 - a x} \qquad x > 0 \quad 0 < a < 1 \tag{A1}$$

replace a by $ae^{j\phi}$:

$$\sum_{n=0}^{\infty} a^n e^{jn\phi} x^n = \frac{1}{1 - a x e^{j\phi}} = \frac{1 - a x e^{-j\phi}}{1 - 2a x \cos(\phi) + a^2 x^2} \tag{A2}$$

Equating real and imaginary parts gives the desired results:

$$\sum_{n=0}^{\infty} a^n x^n \cos(n\phi) = \frac{1 - a x \cos(\phi)}{1 - 2a x \cos(\phi) + a^2 x^2} \tag{A3}$$

$$\sum_{n=0}^{\infty} a^n x^n \sin(n\phi) = \frac{+a x \sin(\phi)}{1 - 2a x \cos(\phi) + a^2 x^2} \tag{A4}$$

Also, from (A1),

$$\sum_{n=1}^{\infty} a^n x^n = \frac{a x}{1 - a x} \tag{A5}$$

Integrating from $-\infty$ to x gives

$$\sum_{n=1}^{\infty} \frac{a^n x^n}{n} = -\ln(1 - a x) \tag{A6}$$

Replacing a by $ae^{j\phi}$ and equating real parts gives

$$\sum_{n=1}^{\infty} \frac{a^n x^n}{n} \cos(n\phi) = -\frac{1}{2} \ln\{1 - 2a x \cos(\phi) + a^2 x^2\} \tag{A7}$$

Acknowledgments. The work reported here was supported by contract DAAG29-76-C-0331 between the Department of the Army and The Ohio State University Research Foundation.

REFERENCES

Bowman, J. J., T. B. A. Senior, and P. L. E. Uslenghi (1969), *Electromagnetic and Acoustic Scattering by Simple Shapes*, North-Holland, Amsterdam.

Felsen, L. B., and N. Marcuvitz (1973), *Radiation and Scattering of Waves*, Prentice-Hall, Englewood Cliffs, N.J.

Lee, S. W. (1972), Comments on 'On a new condition for physical realizability of planar antennas,' *IEEE Trans. Antennas Propagat., AP-20*, 113–114.

Newman, E. H., and D. M. Pozar (1978), Electromagnetic modeling of composite wire and surface geometries, *IEEE Trans. Antennas Propagat., AP-26*, 784–789.

Rhodes, D. R. (1971), On a new condition for physical realizability of planar antennas, *IEEE Trans. Antennas Propagat., AP-19*, 162–166.

Tai, C. T. (1971), *Dyadic Green's Functions in Electromagnetic Theory*, Intext, Scranton, Pa.

Tai, C. T. (1973), Eigen-function expansion of dyadic Green's functions, *Math Note 28*, Radiat. Lab., Univ. of Mich., Ann Arbor.

APPENDIX D

CONSIDERATIONS FOR EFFICIENT WIRE/SURFACE MODELING*

BY

E. H. Newman and D. M. Pozar

The Ohio State University ElectroScience Laboratory
Department of Electrical Engineering
Columbus, Ohio 43212

May 1979

ABSTRACT

The most significant aspects of a moment method surface patch/wire formulation are speed, accuracy, convergence, and versatility. Techniques for improving these parameters are discussed and applied to a solution based on the piecewise sinusoidal reaction formulation.

*The work reported in this paper was supported in part by Grant No. DAAG29-76-G-0331 between the Department of the Army, U. S. Army Research Office and The Ohio State University Research Foundation.

I. INTRODUCTION

In a previous paper [1] the authors presented a moment method solution for wires, rectangular plates, and wire/plate attachments. The purpose of this paper is to present some details of the formulation and of the computer code, and especially to show how the choice of integral equation and expansion and testing functions impact on the versatility, accuracy, computational efficiency, and ease of use of this and other similar formulations.

Briefly, the solution [1] is based on the reaction integral equation and employs speed-of-light piecewise-sinusoidal (PWS) wire, surface, and attachment dipole expansion modes which are placed on the composite wire/surface geometry in an overlapping array such that continuity of current is enforced. The weighting or test modes are chosen identical to the expansion modes, and thus the solution is a Galerkin method, yielding a symmetric impedance matrix. Electric test sources are used, so open as well as closed surfaces can be treated.

II. MODE LAYOUT

The mode layout will be described with the aid of an example, a monopole on a bent plate as shown in Figure 1. The details of the modes have been given previously [1]. Since this problem involves wire, plate, and attachment modes, the impedance matrix, [Z], can be symbolically shown as:

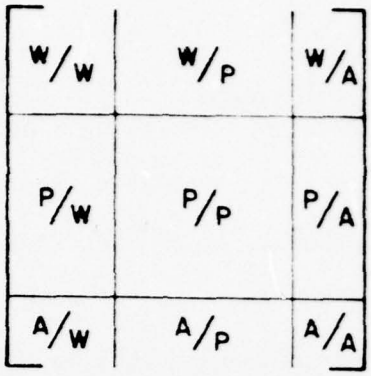

W = WIRE

P = PLATE

A = ATTACHMENT

Wire Modes

Figure 2a shows the wire broken into three segments, or two PWS dipole modes [2]. Note that while the wire current generally does not vanish at the attachment point, the wire mode current does. Thus the need for an attachment mode, described below.

Surface Modes

In the computer code a rectangular plate is defined by specifying the coordinates of three consecutive corners, and the plate segmentation in the two orthogonal directions. Figure 2b shows plate 1 of the bent plate geometry divided into three segments in the 1-to-2 direction and three segments in the 2-to-3 direction. Six overlapping PWS surface dipoles are shown as arrows in the 1-to-2 direction, and six in the 2-to-3 direction. Not shown are the modes on plate 2.

Attachment Modes

The purpose of the attachment mode is to establish continuity of current at the wire/plate junction and also to insure the proper $1/\rho$ singularity of the plate surface current density in the vicinity

of the attachment point. Figure 2c shows the PWS attachment dipole consisting of a circular disk monopole with $1/\rho$ surface current density, and a wire monopole with non-zero current at the attachment point. The attachment point must be at least 0.1λ from the edge of a plate, but it need not be at the center, at a corner, or have any special location with respect to the surface dipole modes.

Overlap Modes

When two plates intersect additional surface-patch dipole modes are required to allow a nonzero continuous current at the plate-to-plate junction. These modes are termed overlap modes. They are identical to the surface dipoles on plates 1 or 2, except that the dipole angle may differ from 180°. Figure 2d shows two overlap modes at the junction of the bent plate. The edges of the overlap surface dipoles need not coincide with the edges of the surface dipole modes on plate 1 or 2, thus allowing the intersection of plates of different size. The code automatically checks to see which plates intersect and inserts the overlap modes.

Toeplitz-Like Properties

The plate-to-plate block of the impedance matrix is shown below:

P_1/P_1	P_1/P_2	P_1/O
P_2/P_1	P_2/P_2	P_2/O
O/P_1	O/P_2	O/O

P_1 = PLATE 1

P_2 = PLATE 2

O = OVERLAP

The various partitions show plate 1-to-plate 1 surface dipole mutual impedances, plate 1-to-plate 2 mutuals, overlap-to-plate 1 mutuals, etc. Due to the regular nature of the placement of surface dipole modes on a plate, considerable savings in computation time is available in computing the plate 1-to-plate 1 block and the plate 2-to-plate 2 block. For example, consider the plate 1-to-plate 1 block, for which the modal layout is shown in Figure 2b. Note that $Z_{1,2} = Z_{3,4}$, $Z_{1,4} = Z_{3,6}$, $Z_{1,11} = -Z_{4,8}$, etc. On an arbitrary plate it is only necessary to compute the mutual impedances between the first mode in the 1-to-2 direction and all the modes on the plate, and the mutuals between the first mode in the 2-to-3 direction and all 2-to-3 modes on the plate. The detail of the plate 1-to-plate 1 block is shown below:

	1	2	3	4	5	6	7	8	9	10	11	12
1	X	O	O	O	O	O	O	O	O	O	O	O
2	X	O	O	O	O	O	O	O	O	O	O	O
3	X	O	O	O	O	O	O	O	O	O	O	O
4	X	O	O	O	O	O	O	O	O	O	O	O
5	X	O	O	O	O	O	O	O	O	O	O	O
6	X	O	O	O	O	O	O	O	O	O	O	O
7	X	O	O	O	O	O	X	O	O	O	O	O
8	X	O	O	O	O	O	X	O	O	O	O	O
9	X	O	O	O	O	O	X	O	O	O	O	O
10	X	O	O	O	O	O	X	O	O	O	O	O
11	X	O	O	O	O	O	X	O	O	O	O	O
12	X	O	O	O	O	O	X	O	O	O	O	O

X = ELEMENT COMPUTED

O = ELEMENT NOT COMPUTED

The x represents elements which must be computed, and the 0 represents elements which can be obtained from the toeplitz-like properties. If on a given plate there are N_{12} modes in the 1-to-2 direction and N_{23}

modes in the 2-3 direction, then only $N_{12} + ? N_{23}$ of the $(N_{12} + N_{23})^2$ elements need to be computed.

III. COMPUTATIONAL ADVANTAGES OF MODE CHOICE

Convergence

A rapidly convergent set of modes will minimize the size and thus the time required to compute the impedance matrix and the required storage. Figure 3 shows a comparison of the input admittance of a monopole on a small plate computed using 15 PWS modes to that using 68 pulse modes [3]. Noting that 15 PWS modes show better agreement with measurements than 68 pulse modes, it is clear that the PWS basis converges relatively fast.

Computation of Impedance Elements

Two algebraically equivalent, but numerically different, techniques for evaluating the elements will be presented, and their relative advantages in computing various elements described. The discussion below will concentrate on surface-to-surface dipole and disk-to-surface dipole impedances which occupy the majority of the time in the computation of the upper triangular part of the symmetric impedance matrix.

A general impedance matrix element Z_{mn} is defined as [1]

$$Z_{mn} = - \int_{e_1} \int_{e_2} \bar{E}_m(e_1,e_2) . \bar{J}_n(e_1,e_2) de_1 de_2, \qquad (1)$$

where e_1, e_2 are independent coordinates on the surface of the n-th expansion mode. $\bar{J}_n$ is the current density of the n-th expansion mode, and $\bar{E}_m$ is the free-space electric field of the m-th test mode, which can be written as

$$\bar{E}_m(e_1,e_2) = \int_{t_1}\int_{t_2} \bar{\bar{G}}_o(e_1,e_2;t_1,t_2).\bar{J}_m(t_1,t_2)dt_1dt_2, \qquad (2)$$

where $\bar{J}_m$ is the current density of the m-th test mode, t_1 and t_2 are independent coordinates on the surface of the m-th test mode, and $\bar{\bar{G}}_o$ is the free-space Green's function. Equations (1) and (2) show that an impedance element in general requires a 4-fold integration, i.e., two to find $\bar{E}_m$ and two to integrate over the surface of the n-th expansion mode. A useful property of the PWS modes is that $\bar{E}_m$ is known in closed form for a wire [4] or a surface [5] monopole, and requires only one simple numerical integration for a disk monopole. Each dipole-to-dipole Z_{mn} is the sum of four monopole-to-monopole impedances.

The second way of computing the impedance elements is to consider the surface-dipole mode current and disk monopole current as being made up of PWS filaments. The order of integration in Equations (1) and (2) can be interchanged to give

$$Z_{mn} = \int_{e_2}\int_{t_2} z_{mn}(e_2,t_2)de_2dt_2, \qquad (3)$$

where $z_{mn}(e_2,t_2)$ represents the mutual impedance between two filaments lying in e_1 and t_1 directions. That is,

$$z_{mn}(e_2,t_2) = -\int_{e_1} \bar{J}_n(e_1,e_2).\int_{t_1} \bar{\bar{G}}_o(e_1,e_2;t_1,t_2).\bar{J}_m(t_1,t_2)dt_1de_1 \ . \qquad (4)$$

An advantage of the PWS modes is that the $z_{mn}(e_2,t_2)$ of Equation (4) are known in closed form [6].

An advantage of the second method, similar to that employed by Popovic and Popovic [7], occurs when computing the impedances between two surface patch monopoles if either the surface current directions are parallel, or the vector transverse to the surface monopoles are parallel. If the expansion and test surface monopoles are each represented by M filaments, then Equation (3) requires M^2 evaluations of $z_{mn}(e_2,t_2)$. However, no more than 2M of the z_{mn} are different. By storing the 2M values prior to computing the mutual impedance, the computation time will be proportional to 2M rather than M^2.

Another time-saving technique deals with the slow convergence of the numerical integration of Equation (3) when computing the mutual impedance of two touching surface monopoles. This slow convergence is a result of the fact that the imaginary part of the mutual impedance of two PWS filaments has a logarithmic singularity as the distance between the two filaments gets small [8]. For small separation x, the reactance between two filaments can be written as [8]

$$X(x) = C_1 + C_2 \ln(x). \tag{5}$$

The constants C_1 and C_2 can be easily evaluated and the logarithmic singularity integrated analytically. Figure 4 shows the self-reactance of a surface monopole computed using Equation (1), Equation (3) directly, and Equation (3) with the above two techniques (i.e., only M evaluations of z_{mn} and extracting logarithmic singularity). Also shown is the computation time for each of the three methods; all times shown in this

paper are for the Datacraft 6024 which is about an order of magnitude slower than an IBM370-165. In using Equations (1) and (3) directly the surface monopoles are separated by $10^{-4}\lambda$ to avoid the singularity. No separation is required if the logarithmic singularity is removed. From Figure 4 it can be seen that not only is the use of Equation (3) with the above discussed two techniques faster than the other methods, but it is also more accurate.

One case where Equation (1) has an advantage occurs when computing the mutual impedance between a disk monopole (of an attachment mode) and the set of surface dipoles on a plate which is parallel to the plane of the disk. Here, advantage can be taken of the fact that only the E_ρ field of the disk monopole is needed (since $E_\phi=0$ and $E_z\ \hat{z}.\bar{J}_n=0$), and also E_ρ is independent of ϕ. Thus, much time can be saved by filling a table of values of E_ρ versus ρ. This table can then be interpolated to find $\bar{E}_m$ on every surface dipole mode on the plate, making the evaluation of Equation (1) very fast. An order of magnitude saving in computer time is then realized for small plates, with substantially greater savings for larger plates.

V. CONCLUSION

This paper has demonstrated that in a moment method surface/wire formulation, the piecewise sinusoidal modes have significant advantages from the standpoints of convergence and the fast and accurate computation of the impedance matrix. Also, techniques for reducing the run time of surface/wire codes were presented. To show how the speed of a typical solution can be improved by these methods, the problem of a $\lambda/4$ monopole

mounted on a 1.0λ square plate was run without using any of the techniques mentioned in this paper, and again using all of the mentioned techniques. Using the techniques decreased the run time by a factor of twenty to 115 sec. on the Datacraft 6024 (about 20 sec. on IBM 370-165), with an increase in accuracy (both runs used the symmetry of the impedance matrix).

Acknowledgment

The authors would like to thank Professor J.H. Richmond for supplying invaluable suggestions, advice and computer subroutines. Helpful discussions with Dr. W.D. Burnside and Dr. N.W. Wang are also appreciated.

REFERENCES

1. E. H. Newman and D. M. Pozar, "Electromagnetic Modeling of Composite Wire and Surface Geometries," IEEE AP-26, pp. 784-789, November 1978.

2. Y. T. Lin and J. H. Richmond, "EM Modeling of Aircraft at Low Frequencies," IEEE AP-23, pp. 53-56, January 1975.

3. A. W. Glisson, "On The Development of Numerical Techniques for Treating Arbitrarily-shaped Surfaces," Dissertation, University of Mississippi, June 1978.

4. S. A. Schelkunoff and H. T. Friis, Antennas: Theory and Practice, Wiley, 1952.

5. J. H. Richmond, D. M. Pozar and E. H. Newman, "Rigorous Near-zone Field Expressions for Rectangular Sinusoidal Monopole," IEEE AP-26, p. 509, May 1978.

6. J. H. Richmond and N. H. Geary, "Mutual Impedance of Non-planar-skew Sinusoidal Dipoles," IEEE AP-23, May 1975.

7. Z. D. Popovic and B. D. Popovic, "Transformation of Double Integrals Appearing in Variational Formulation of Cylindrical Antenna Problems," publications De la Faculte Dielectrotechnique de L'Universite A., Belgrade, Serie: Electronique, Telecommunications Automatique, No. 64, 1971.

8. W. A. Imbriale and P. G. Ingerson, "On Numerical Convergence of Moment Solutions of Moderately Thick Wire Antennas Using Sinusoidal Basis Functions," IEEE AP-21, pp. 363-366, May 1973.

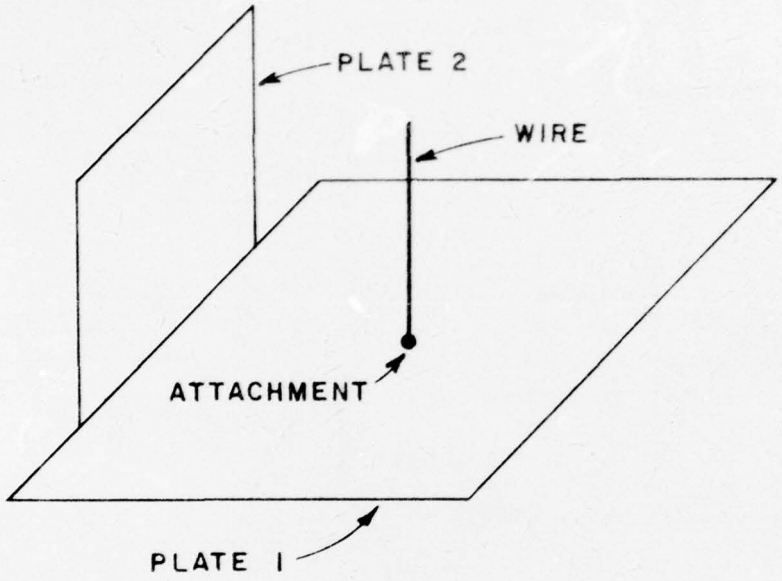

Figure 1. Geometry for the monopole on a bent plate.

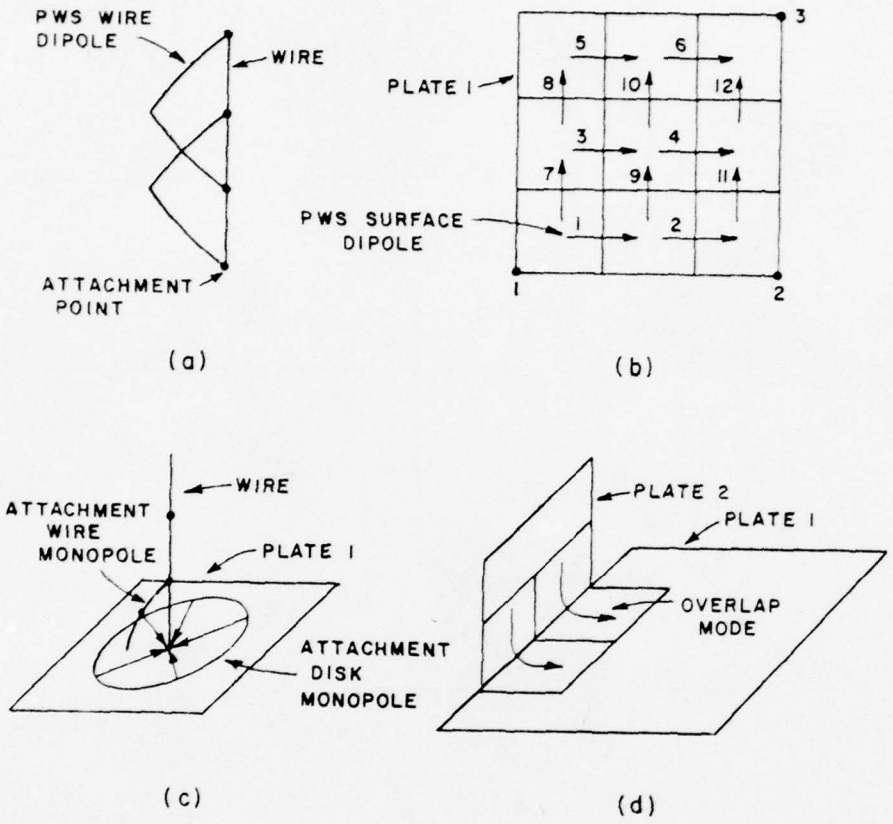

Figure 2. Layout of the (a) wire, (b) surface dipole, (c) attachment, and (d) overlap modes for a monopole on a bent plate.

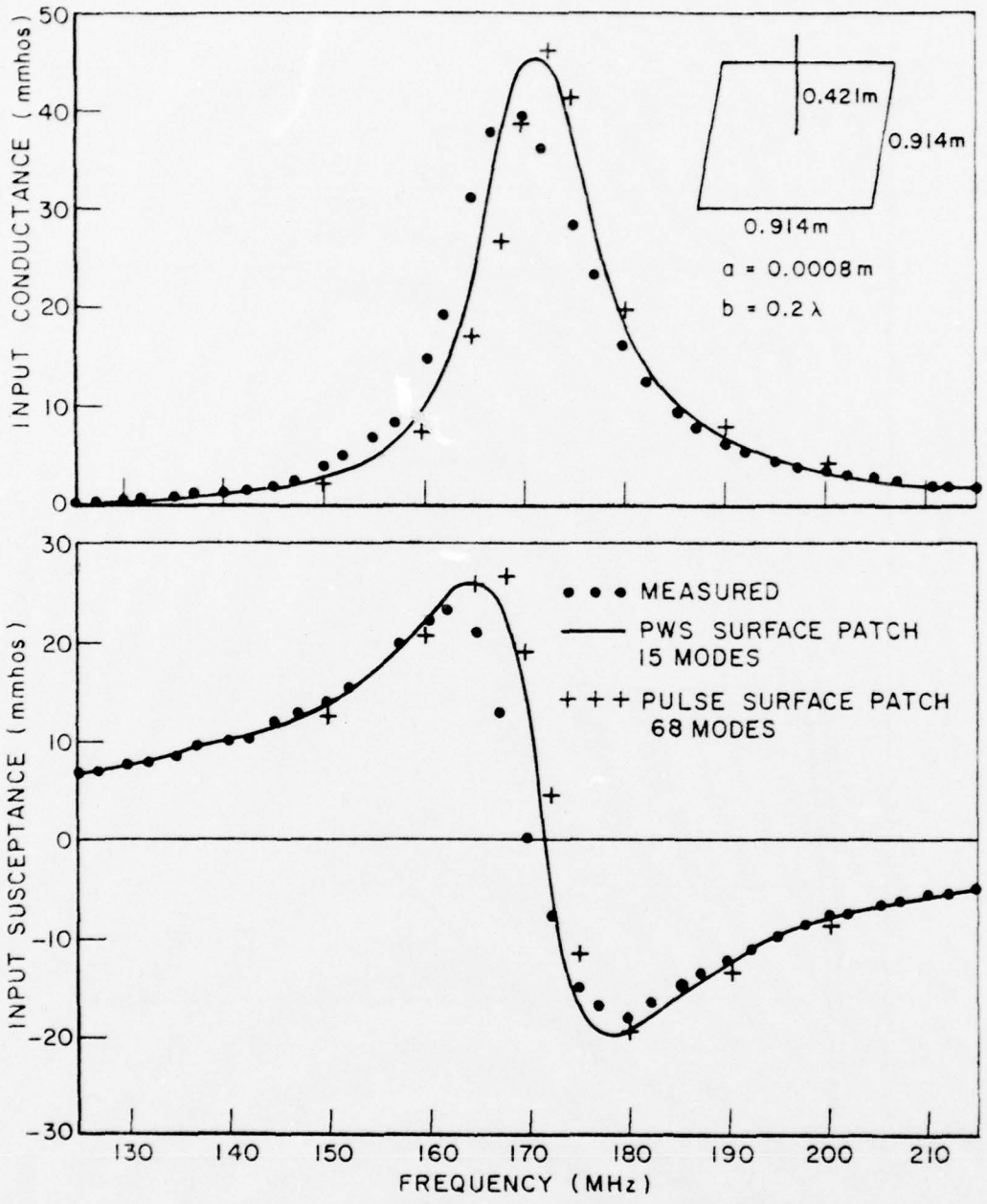

Figure 3. A comparison of measured input impedance of a monopole on a small plate with that computed using PWS modes and pulse modes.

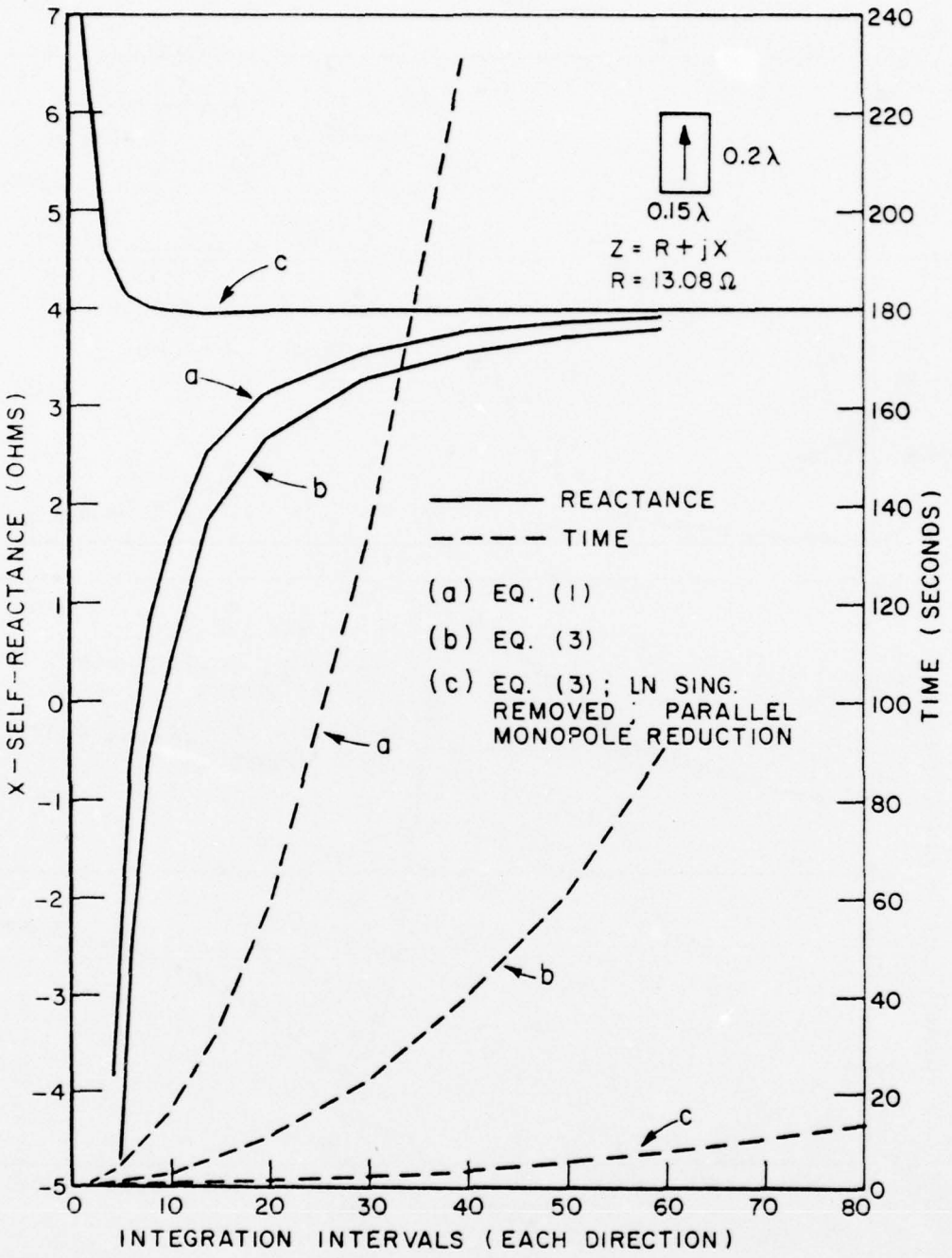

Figure 4. Self-reactance and computation time for a .15λ by .2λ surface monopole computed three ways.

APPENDIX E

ANALYSIS OF A MONOPOLE MOUNTED NEAR OR AT THE EDGE OF A HALF-PLANE*

D. M. Pozar and E. H. Newman

The Ohio State University ElectroScience Laboratory
Department of Electrical Engineering
Columbus, Ohio 43212

ABSTRACT

The problem of a monopole antenna mounted near or at the edge of a half-plane is solved using a hybrid moment method solution with an integral expression for the exact half-plane Green's function. Results are presented for input impedance of a $\lambda/4$ monopole vs. distance from the half-plane edge, and vs. angle for an edge-mounted antenna. Simple expressions for the surface current density induced on the halfplane are derived and used to synthesize an attachment mode for use with the author's previously developed surface patch moment method solution when a wire is attached at or near an edge of a finite plate.

---

*The work reported in this paper was supported in part by Grant DAAG29-76-G-0331 between the U. S. Army Research Office, Research Triangle Park, North Carolina and The Ohio State University Research Foundation, Columbus, Ohio

I. INTRODUCTION

A problem of continued interest is that of antennas mounted on finite conducting bodies. Antennas on spherical bodies have been analyzed[1], as well as antennas on more general structures[2,3]. The authors have previously[4] presented a surface patch moment method solution for geometries involving wires and rectangular plates, including plate/plate and wire/plate junctions, where the wire/plate attachment point was restricted to be .1λ or more from a plate edge. This paper presents a new wire/plate attachment mode that removes this restriction, allowing a wire to be attached close to or on a half-plane type edge. The development of this new surface patch moment method expansion mode is based on the canonical solution of a vertical monopole mounted near or at the edge of a perfectly-conducting half-plane. This canonical solution is a hybrid moment method using the exact half-plane Green's function in integral form, with the source and image terms separated from the diffracted field. This form of the Green's function also yields the near zone surface current density on the half-plane in the vicinity of the edge and source, which is used to synthesize the above-mentioned surface patch expansion mode for attachments near or at an edge. Presented are graphs of input impedances for a vertical $\lambda/4$ monopole vs. distance from a half-plane edge, and for a $\lambda/4$ monopole mounted on a half-plane edge vs. azimuth angle. Far-field results for antennas near half-plane edges are available in[5].

The problem of a wire antenna in free space can be solved via the moment method solution of an integral equation using the free space Green's function[6]. If the wire antenna is in the presence of another scattering structure there are two possible modifications. The first is to replace the free-space Green's function by the special Green's function for the particular scattering structure. The second approach is to retain the free-space Green's function, but suitably

expand the currents on the wire and the scattering structure, and solve for the expansion coefficients in the MM solution. The advantage of the first approach is that no new unknowns are introduced into the MM solution and the size of the impedance matrix does not increase over that of the isolated wire, while the disadvantage is that the Green's function of the scatterer must be known in a computationally efficient form. The advantage of the second approach is that the Green's function of the scatterer need not be known, while the disadvantage is that new unknowns are introduced and the size of the required impedance matrix can increase substantially if the scatterer is electrically large. (Note that the MM/GTD hybrid method[2] can be considered to be of the first type, where the exact Green's function is replaced by the GTD or high-frequency approximation.) Both approaches are used in this paper.

II. SOLUTION FOR VERTICAL MONOPOLE NEAR EDGE OF HALF-PLANE USING EXACT GREEN'S FUNCTION

Theory

The geometry of the problem is shown in Figure 1. The wire and half-plane are considered to be perfectly-conducting. The basic idea of the solution is to expand the wire currents using piecewise-sinusoidal modes, find the fields of test modes (also PWS) in the presence of the half-plane, and compute an impedance matrix:

$$Z_{ij} = - \int_{y_j} I_j(y) \int_{y_{oi}} I_i(y_o) E_y (y|y_o) dy_o dy \qquad (1)$$

where $I_i(y)$ is the PWS test/expansion mode current,

$E_y(y|y_o)$ is the half-plane Green's function, representing the E_y field due to a y infinitesimal electric dipole of unit moment.

Since the test and expansion modes are equivalent we have a Galerkin solution, and $Z_{ij}=Z_{ji}$. The wire currents and input impedance then follow from the solution of a matrix equation of the form $\left[Z\right]\left[I\right] = \left[V\right]$, where $\left[Z\right]$ is the impedance matrix, $\left[I\right]$ is the column vector of current expansion coefficients, and $\left[V\right]$ is the vector of mode voltages.

Thus, this solution depends upon the availability of the half-plane Green's function in a form suitable for fast and accurate evaluation. It was first attempted to use the familiar form of the half-plane Green's function expressed as an eigenfunction expansion, such as given by Tai[5]. This representation was found to be unsuitable for two reasons. First, the eigenfunction expansion contains an infinite series of infinite integrals that contain source and image singularities that would make evaluation of self or overlapping mutual impedance terms difficult to do accurately. Second, the eigenfunction representation does not lend itself to small argument approximations for evaulation of near zone surface currents in simple closed form. It was found that the first term of the series would give the correct edge behavior, but not the correct source singularity. For these reasons, an integral expression for the half-plane Green's function given by Senior[7] was used.

From[7], the total E_y field due to a $\hat{y}$ directed infinitesimal electric dipole of moment $I\ell$ in the presence of a conducting half-plane is ($e^{j\omega t}$ time dependence)

$$E_y = \frac{I\ell Z_o}{4\pi j}\left\{\frac{-jk}{\sqrt{\rho\rho_o}}\cos\frac{\phi}{2}\cos\frac{\phi_o}{2}H_o^{(2)}(kR_1) + \frac{j}{2}\left(\frac{\partial^2}{\partial y\partial y_o} - k^2\right)I_R - \frac{j}{2}\left(\frac{\partial^2}{\partial y\partial y_o} + k^2\right)I_R'\right\} \tag{2}$$

where

$$I_R = \int_{-\mu_R}^{\infty} H_1^{(2)}(kR\cosh u)du \tag{3}$$

Defining the modified Hertz potentials

$$\pi^{dR} = \frac{j}{2} \int_{\mu_R}^{\infty} H_1^{(2)}(kR \cosh u)du; \tag{12}$$

$$\pi^{dR'} = \frac{j}{2} \int_{\mu_{R'}}^{\infty} H_1^{(2)}(kR' \cosh u)du, \tag{13}$$

and using the relation[7]

$$\int_{-\infty}^{\infty} H_1^{(2)}(kR \cosh u)du = 2j \frac{e^{-jkR}}{kR}, \tag{14}$$

and the fact that $\frac{\partial R}{\partial y_o} = -\frac{\partial R}{\partial y}$ and $\frac{\partial R'}{\partial y_o} = \frac{\partial R'}{\partial y}$, allows the diffracted field to be written as

$$E_y^{dif} = \frac{I\ell Z_o}{4\pi j}\left\{\frac{-jk}{\sqrt{\rho\rho_o}} \cos\frac{\phi}{2} \cos\frac{\phi_o}{2} H_o^{(2)}(kR_1) - \left(\frac{\partial^2}{\partial y \partial y_o} - k^2\right)\pi^{dR} + \left(\frac{\partial^2}{\partial y \partial y_o} + k^2\right)\pi^{dR'}\right\}, \tag{15}$$

where $E_y = E_y^{inc} + E_y^{ref} + E_y^{dif} = E_y^{g.o.} + E_y^{dif}$.

Note that, using Equation (14), π^{dR} and $\pi^{dR'}$ can be expressed in terms of finite integrals:

$$\pi^{dR} = -\frac{1}{2}\frac{e^{-jkR}}{kR} - \frac{j}{2}\int_{o}^{\mu_R} H_1^{(2)}(kR \cosh u)du, \tag{16}$$

$$\mu^{dR'} = -\frac{1}{2}\frac{e^{-jkR'}}{kR'} - \frac{j}{2}\int_{o}^{\mu_{R'}} H_1^{(2)}(kR' \cosh u)du. \tag{17}$$

Defining the modified Hertz potentials

$$\pi^{dR} = \frac{j}{2} \int_{\mu_R}^{\infty} H_1^{(2)}(kR \cosh u)du; \tag{12}$$

$$\pi^{dR'} = \frac{j}{2} \int_{\mu_{R'}}^{\infty} H_1^{(2)}(kR' \cosh u)du, \tag{13}$$

and using the relation[7]

$$\int_{-\infty}^{\infty} H_1^{(2)}(kR \cosh u)du = 2j \frac{e^{-jkR}}{kR}, \tag{14}$$

and the fact that $\frac{\partial R}{\partial y_o} = -\frac{\partial R}{\partial y}$ and $\frac{\partial R'}{\partial y_o} = \frac{\partial R'}{\partial y}$, allows the diffracted field to be written as

$$E_y^{dif} = \frac{I\ell Z_o}{4\pi j}\left\{\frac{-jk}{\sqrt{\rho\rho_o}} \cos\frac{\phi}{2}\cos\frac{\phi_o}{2} H_o^{(2)}(kR_1) - \left(\frac{\partial^2}{\partial y \partial y_o} - k^2\right)\pi^{dR} + \left(\frac{\partial^2}{\partial y \partial y_o} + k^2\right)\pi^{dR'}\right\}, \tag{15}$$

where $E_y = E_y^{inc} + E_y^{ref} + E_y^{dif} = E_y^{g.o.} + E_y^{dif}$.

Note that, using Equation (14), π^{dR} and $\pi^{dR'}$ can be expressed in terms of finite integrals:

$$\pi^{dR} = -\frac{1}{2}\frac{e^{-jkR}}{kR} - \frac{j}{2}\int_0^{\mu_R} H_1^{(2)}(kR \cosh u)du, \tag{16}$$

$$\mu^{dR'} = -\frac{1}{2}\frac{e^{-jkR'}}{kR'} - \frac{j}{2}\int_0^{\mu_{R'}} H_1^{(2)}(kR' \cosh u)du. \tag{17}$$

It can be shown that π^{dR} and $\pi^{dR'}$ are not singular at R=0 or R'=0. The diffracted electric field is now in a form which has no singularities at the source or image.

Since the geometrical optics terms have been separated from the diffracted field, the impedance matrix $[Z]$ can, for computational purposes, be broken into two parts; $[Z] = [Z_o] + [\Delta Z]$, where $[Z_o]$ represents the impedance matrix of a monopole on an infinite ground plane ($E_y^{g.o.}$ contribution) and $[\Delta Z]$ represents the E_y^{dif} field contribution which accounts for the edge. Since PWS modes are used for expansion and testing the $[Z_o]$ elements can be computed in closed form[8], eliminating the difficulties which would be encountered if this evaluation were done numerically. This is an important and useful distinction from other similar solutions[1]. The remaining task is to evaluate $[\Delta Z]$.

The PWS modes are arranged on the wire as shown in Figure 2, numbered from top to bottom. The test modes are positioned on the wire axis at $(x_o, z=0)$ while the expansion modes are placed on the wire surface at $(x_o, z=a)$, where a is the wire radius. Note that the modes are PWS dipoles except for the bottom mode, which is a PWS monopole with its terminal at the base of the wire. This allows non-zero current at the attachment point. The contribution to the mutual impedance between modes i and j due to the diffracted field can then be written as

$$\Delta Z_{ij} = - \int_{y_{oi}} I_i(y_o) \int_{y_j} I_j(y) E_y^{dif}(y|y_o)\, dy\, dy_o. \qquad (18)$$

Thus, $[\Delta Z]$ can be calculated with two numerical integrations for Equation (18) and one for Equations (16) and (17). These integrations are well behaved, typically requiring only 10-20 Simpson intervals each. This ease of computation

of $[\Delta Z]$ is a direct result of the fact that the incident and reflected field components were separated from the total field, allowing the nearly singular portion, $[Z_o]$, to be evaluated in closed form.

The solution described above gave a quickly converging result for the wire currents, as shown in Table I below. This table gives $\Delta Z = Z_{in} - Z_o$, where Z_{in} is the input impedance of a $\lambda/4$, $a=.001\lambda$ monopole near the edge of a half-plane, and Z_o is the input impedance of the same antenna mounted on an infinite ground plane. x_o is the distance of the antenna from the edge. Results are shown for 1, 2, and 3 modes on the monopole. A delta gap generator at the base of the monopole was used.

Table I

x_o/λ	ΔZ, 1 mode	ΔZ, 2 modes	ΔZ, 3 modes
.05	12.1-j7.1Ω	11.8-j8.7Ω	11.7-j9.0Ω
.10	4.2-j8.2Ω	3.5-j9.2Ω	3.3-j9.4Ω
.20	-2.8-j3.8Ω	-3.6-j3.8Ω	-3.7-j3.8Ω
.40	-.32+j1.9Ω	-.09+j2.2Ω	-.04+j2.2Ω
.60	.87-j.73Ω	.85-j.91Ω	.85-j.95Ω

The convergence of Z_o is shown in Table II below:

Table II

Modes	Z_o
1	36.5+j21.1Ω
2	40.6+j20.6Ω
3	41.4+j21.00Ω
4	41.7+j21.3Ω

From the above data it is seen that the solution has practically converged with two wire modes. Computation time for this solution is about 30 seconds* when 2 expansion modes are used. This solution is valid for any distance, x_o, from the half-plane edge except when the antenna is within a few wire radii of the edge. In this case numerical problems are encountered since the fields contain the $1/\sqrt{x}$ edge singularity. Plots of Z_{in} vs. x_o are shown in Figures 3 and 4, where comparison is made with results from the MM/GTD method[2], and with results from the MM/surface patch solution presented in the next section.

ϕ-variation of wire current

The solution in the previous section used an axial current filament for testing and a circumferentially uniform surface current located on the surface of the wire for expansion. Thus, the solution did not account for or give any information about the circumferential variation of the current around the wire surface. This aspect of the solution was of interest for two reasons.

First, it was important to determine if a full account of the circumferential variation of the wire current, due to the edge proximity, would alter the input impedance as determined by the previous solution, which did not account for any variation. Secondly, it was of interest to determine the circumferential variation of the current at the base of the wire in order to build a suitable expansion mode for wires attached near an edge, for use in the surface patch MM solution.

*All times reported here are for Datacraft 6024 - about 8 times slower than IBM 360/165.

The circumferential variation of the axial wire current was taken into account by placing expansion filaments evenly around the surface of the wire, i.e., by constructing a wire-grid model of the wire[9]. Each filament is an independent unknown, and can also be broken up into separate modes along its length. Test modes are placed alongside the expansion filaments spaced .000001λ away. This procedure approximates true surface testing and expansion.

Figure 5 shows a λ/4 monopole, radius .001λ, placed .05λ from the edge of a half-plane. Also shown are the positions of eight expansion filaments used in this example. In this example 3 modes were employed in the longitudinal direction for a total of 8x3 = 24 unknowns.

The current at the base of the monopole is plotted as magnitude and phase in Figure 5. As expected, the data show symmetry between filaments 2, 3, 4 and 8, 7, 6, respectively. The data also show, as might be expected, more current flowing away from the edge than toward it. If the filament currents in the above table are added to find the total current, the "average" input impedance can be calculated and is found to be identical to the value given by the simpler one-filament solution of section B. This interesting effect occurs for other segmentation schemes and distances from the edge, and is similar to an effect reported in connection with closely spaced wire antennas[9]. The circumferential variation of the wire current becomes less pronounced as one moves up the wire.

Expressions for surface currents

In this section simple closed form expressions will be derived for the surface current density on a perfectly-conducting half-plane induced by an infinitesimal electric dipole on the surface of the halfplane and near its edge. These results will be used for synthesis of an expansion mode for a wire attachment near an edge in the surface patch MM solution.

For the total surface current density, one must vectorally add the currents on the top of the half-plane ($\phi=0$, $\hat{n}=\hat{y}$) to those on the bottom of the half-plane ($\phi=2\pi$, $\hat{n}=-\hat{y}$):

$$J_{sx} = H_z(\phi=0)-H_z(\phi=2\pi), \tag{19}$$

$$J_{sz} = - H_x(\phi=0)+H_x(\phi=2\pi). \tag{20}$$

The total exact H fields are, from[7],

$$H_x = \frac{I\ell}{4\pi j}\left\{\frac{k(z-z_o)}{R_1\sqrt{\rho\rho_o}}\cos\frac{\phi}{2}\cos\frac{\phi_o}{2}\,H_1^{(2)}(kR_1) + \frac{k}{2}\frac{\partial I_R}{\partial z_o} + \frac{k}{2}\frac{\partial I_{R'}}{\partial z_o}\right\}, \tag{21}$$

$$H_z = \frac{I\ell}{4\pi j}\left\{\frac{-k}{2}\frac{\partial I_R}{\partial x_o} - \frac{k}{2}\frac{\partial I_{R'}}{\partial x_o}\right\} \tag{22}$$

Since the dipole is located on the top surface of the half-plane at $y_o=z_o=0$, we have $\phi_o=0$, $R=R'$, $\mu_R=\mu_{R'}$, and $I_R=I_{R'}$. Thus, from (19)-(22),

$$J_{sx} = \frac{I\ell}{4\pi j}\left\{-k\left.\frac{\partial I_R}{\partial x_o}\right|_{\phi=0} + k\left.\frac{\partial I_R}{\partial x_o}\right|_{\phi=2\pi}\right\} \tag{23}$$

$$J_{sz} = \frac{I\ell}{4\pi j}\left\{\frac{-2kz}{R_1\sqrt{\rho\rho_o}}\,H_1^{(2)}(kR_1) - k\left.\frac{\partial I_R}{\partial z_o}\right|_{\phi=0} + k\left.\frac{\partial I_R}{\partial z_o}\right|_{\phi=2\pi}\right\}. \tag{24}$$

Now let $\alpha=\sinh^{-1}\left\{\frac{2\sqrt{\rho\rho_o}}{R}\right\}$, then

$$\mu_R\Big|_{\phi=0} = \alpha = -\mu_R\Big|_{\phi=2\pi}, \text{ so}$$

$$I_R\Big|_{\phi=0} - I_R\Big|_{\phi=2\pi} = 2\int_0^{\alpha} H_1^{(2)}(kR\cosh u)\,du$$

$$= 2\psi\,(x,z|x_o,z_o)\Big|_{\phi=\phi_o=0} \tag{25}$$

where

$$\psi(x,z|x_o,z_o) = \int_0^{\mu_R} H_1^{(2)}(kR\cosh u)\,du. \tag{26}$$

Then (23), (24) become

$$J_{sx} = \frac{I\ell}{4\pi j}\left\{-2k\,\frac{\partial}{\partial x_o}\,\psi(x,z|x_o,z_o)\right\} \tag{27}$$

$$J_{sz} = \frac{I\ell}{4\pi j}\left\{-\frac{2kz}{R_1\sqrt{\rho\rho_o}}\,H_1^{(2)}(kR_1) - 2k\,\frac{\partial}{\partial z_o}\,\psi(x,z|x_o,z_o)\right\}. \tag{28}$$

We now develop a small argument approximation for ψ:

For small x,

$$H_1^{(2)}(x) = x/2 + j\,\frac{2}{\pi x},$$

so (26) becomes

$$\psi \cong \int_0^{\mu_R}\left[\frac{kR\cosh u}{2} + \frac{2j}{\pi kR\cosh u}\right]du$$

$$= k\sqrt{\rho\rho_o}\cos\tfrac{1}{2}(\phi-\phi_o) + \frac{2j}{\pi kR}\tan^{-1}\frac{2\sqrt{\rho\rho_o}}{R}\cos\tfrac{1}{2}(\phi-\phi_o). \tag{29}$$

For the present case $\phi=\phi_o=0$, so $\rho=x$ and $\rho_o=x_o$. The real part of the approximation to the function ψ is ignored in the remainder of the analysis since it is negligible in comparison to the imaginary part.

The last step is to carry out the differentiations as indicated in (27),(28). When this is done there will be present terms which vary as $1/R^2$ due to the charges which are located at the ends of the dipole. Since these terms vanish in a physical solution which has continuous current, they are omitted in the final expressions. So, for a vertical electric dipole of moment $I\ell$ near the edge of a halfplane, the surface currents are

$$J_{sx} = \frac{-I\ell}{\pi^2 R_1^2}\left[\sqrt{\frac{x}{x_o}} + \frac{2\sqrt{xx_o}(x-x_o)}{R^2}\right] \text{ A/m} \tag{30}$$

$$J_{sz} = \frac{-I\ell z}{\pi^2 R_1^2}\left[\frac{1}{\sqrt{xx_o}} + \frac{2\sqrt{xx_o}}{R^2}\right] \text{ A/m} \quad . \tag{31}$$

Observe that $J_{sx}\to 0$ with $\sqrt{x}$ dependence and $J_{sz}\to\infty$ with $1/\sqrt{x}$ dependence, as $x\to 0$ as required by edge conditions. Also, J_{sx} and J_{sz} contain the correct $1/R$ singularity in the vicinity of the source. It is also of interest to note that Equations (30), (31) are not frequency dependent, i.e., they are quasi-static results. However, retaining the first term in the real part or higher terms in the imaginary part of (29) will introduce a frequency dependence, if desired. Three-dimensional plots of Equations (30)-(31) are shown in Figures 6 and 7.

III. SURFACE PATCH MM ATTACHMENT MODES FOR WIRE/PLATE ATTACHMENTS NEAR OR AT EDGES

This section deals with methods of modifying the author's surface patch modeling program[4] to handle antennas mounted near or at the edge of plates. Originally, the program used an attachment mode which had the following features:

a) Enforced continuity of current from wire to plate.

b) Enforced the proper $\hat{\rho}/\rho$ dependence for surface current in the vicinity of the attachment point.

c) Had no ϕ-variation in surface current. (In this section ϕ is used to denote azimuthal direction around the attached wire.)

d) Worked well for wire attachments .1λ or further from an edge, and for .1$\lambda \leq b \leq$ .25λ.

This attachment mode, shown in Figure 8a, failed for antennas mounted closer than .1λ from the edge as shown in Figures 3 and 4 (as mode A), probably for the following reasons:

a) Disk mode radius was limited to the distance of the monopole from the edge, thus reducing the area in which the $\hat{\rho}/\rho$ singularity was enforced.

b) Disk mode did not contain any ϕ-variation in current density, which probably becomes increasingly important as the antenna gets closer to the edge.

Thus, a better attachment mode was needed to handle antennas mounted close to or at the edge of plates.

Attachment Mode Development

Four expansion modes, denoted as A,B,C,D, for wire/plate junctions will be described. All four modes consist of a disk monopole which rests on the plate, and a wire monopole which overlaps with the connecting wire. Since this wire monopole is common to all four attachment modes, it is not described in detail here.

Mode A) - This is the original disk monopole described in[4], having a surface current density

$$J_\rho(\rho,\phi) = A\,\frac{\sin k(b-\rho)}{2\pi\rho} \quad , \tag{32}$$

where A is a normalization constant chosen to satisfy (33):

$$\int_{\phi=0}^{2\pi} J_\rho(a,\phi)\,a\,d\phi = 1 \text{ amp} \quad . \tag{33}$$

In (32), a is the wire radius, and b is the outer radius of the disk. For this mode the disk is circular, so b is a constant w.r.t. ϕ. Figure 8a shows how this mode would be applied to a wire attachment near an edge. Mode A) fails when used near an edge for the above mentioned reasons.

Mode B) - The first approach toward improvement of disk mode A) was to maintain the disk radius at about .2λ where it overlapped the plate, but cut off the disk where it overhung the plate; see Figure 8b. The surface current density for this disk mode can be written as

$$J_\rho(\rho,\phi) = B\,\frac{\sin k(b(\phi)-\rho)}{2\pi\rho} \quad , \tag{34}$$

where B is a constant chosen to satisfy (33) and $b(\phi)$ is the outer radius of the disk, now expressed as a function of ϕ.

This type of mode overcomes some of the drawbacks of the previous mode in that it has a ϕ-variation of current and yields a larger area where the $1/\rho$ singularity is enforced. The results obtained when using this mode are not significantly better than those obtained with the original mode A). This is probably due to the fact that the ϕ-dependence is not close enough to the exact dependence. For instance, when ρ is close to a, the current density of mode B) is large but does not vary appreciably with ϕ, while

Figure 5 and Equation (30) show that significantly less current is flowing toward the edge than away from it. Another point is that this mode does not have a uniform limit as the attachment point approaches the edge. One would expect that the current flowing toward the edge would smoothly decrease to zero as the attachment moves to the edge. Mode B) does not have this behavior. The disk modes presented below do have this desired asymmetry.

Mode C) - The next step was to construct a disk mode which had less current flowing toward the edge than away from it. One distribution which does this is

$$J_\rho(\rho,\phi) = C \frac{\sin k(b(\phi)-\rho)}{2\pi\rho} \sin kb(\phi), \qquad (35)$$

where C is a constant chosen to satisfy (33). This current distribution roughly corresponds to that obtained from the exact solution for the circumferential current variation, as shown in Figure 5. This type of mode has the desired property of uniformly approaching a semicircular disk as the attachment point moves to the edge (Figure 8). Also, this mode reduces to the standard attachment mode, mode A), when the distance between the attachment point and edge becomes greater than the disk outer radius ($\sim.2\lambda$), since $b(\phi)$ = constant for this case.

This type of attachment mode gave the best results for antennas at or near an edge. Results from the surface patch MM solution using mode C) with a $\lambda/4$ monopole near the long edge of a $.4\lambda x.5\lambda$ plate are shown in Figures 3 and 4. The shift between the surface patch results and the exact results for a semi-infinite half-plane in these figures is due to the fact that a finite-sized plate had to be used with the former solution. As can be seen, mode C) yields a significant improvement over mode A). Figure 10 shows results using mode C) when the monopole is mounted on the edge of a plate vs. angle.

Mode D) - The next type of disk mode which was developed was one constructed from an arbitrary number of wedge-shaped sectors of current, with current distribution like that of disk mode B) over each sector, but with each sector being an independent unknown. See Figure 8d, which shows a 4 sector disk. This type of mode has the advantage of allowing the MM solution to arrive at currents (both magnitude and phase) which best satisfy the integral equation in a least-mean-square sense. The resolution of the variation in disk current can be made finer by increasing the number of wedge-shaped sectors that the disk is broken into. When eight such sectors were used the results for input impedance agreed fairly well with those obtained using mode C). Note that this type of attachment mode would work well for wires attached to piecewise-curved surfaces.

Edge Mode - Recently, there has been an interest in directly enforcing the edge condition in MM solutions[14]. Thus, it was decided to construct a mode, based on the analysis of Section II, that would enforce the edge singularity of the surface current component parallel to the edge of the half-plane, and study its effect on the solution. This "edge mode" was constructed from PWS current filaments to embody the essential features of Equation (31). The surface current density of this mode is

$$J_s(x,z) = \frac{A}{\sqrt{x}} \begin{cases} \dfrac{-\sin k(z+\ell)}{\sin k(\ell-z_o)} & \text{for } -\ell<z<-z_o, \\ \dfrac{\sin kz}{\sin kz_o} & \text{for } -z_o<z<z_o \\ \dfrac{\sin k(z-\ell)}{\sin k(z_o-\ell)} & \text{for } z_o<z<\ell \end{cases} \qquad (36)$$

where the coordinate system is shown in Figure 1, A is a suitable normalizing constant, and 2ℓ is the overall length of the mode. The width of the mode (extent in x-direction) is arbitrary, but since most of the current is located near the singularity at x=0, this width is not too critical if chosen to be $.05\lambda$ or greater. The result of using this edge mode with different lengths and widths was interesting. First, the edge mode was excited in the surface patch MM solution, as indicated by a non-zero mode current. However, the input impedance did not significantly change from the result obtained without using an edge mode. Thus, all of the other surface patch, wire, and attachment currents changed in the presence of the edge mode in such a way as to leave the input impedance unaltered. At the present time the best explanation we have for this effect is that the singular behavior of the edge current can be approximated adequately in a least-mean-square sense by the surface-patch dipoles alone. Incorporation of a special edge mode explicitly satisfying the edge condition does not improve on this situation in the present case.

IV. SOLUTION FOR A RADIAL MONOPOLE AT THE EDGE OF A HALF-PLANE USING EXACT GREEN'S FUNCTION

Theory

The solution for a monopole mounted at the edge of a half-plane is similar to the solution described in Section II, except that here the exact Green's function is expressed in spherical coordinates. This alleviates the problem of moving the vertical monopole up to the edge, while allowing the monopole to be oriented in a position other than vertical. Figure 9 shows the geometry. The monopole lies in the x-y plane at an angle α from the half-plane surface. Without loss of generality, α is restricted to $0 \leq \alpha \leq \pi$.

From another paper by Senior[12], the radial component of the electric field due to a radially directed electric dipole, with moment $I\ell$, near the edge of a half-plane is

$$E_{rr} = \frac{I\ell Z_o}{4\pi j} \left\{ \frac{-j}{2} \left(\frac{\partial^2}{\partial r_o^2} + k^2 \right) \frac{r_o}{r} (I_R - I_{R'}) \right\} \quad , \tag{37}$$

where I_R and $I_{R'}$ are defined in (3), (4). Equation (37) represents the fields in terms of a Debye potential, whereas Equation (2) represented the fields in terms of a Hertz potential.

Now, it can be shown that

$$E_{rr}^{inc} = \frac{I\ell Z_o}{4\pi j} \left\{ \left(\frac{\partial^2}{\partial r_o^2} + k^2 \right) \frac{r_o}{r} \frac{e^{-jkR}}{kR} \right\} \quad , \text{ and} \tag{38}$$

$$E_{rr}^{image} = - \frac{I\ell Z_o}{4\pi j} \left\{ \left(\frac{\partial^2}{\partial r_o^2} + k^2 \right) \frac{r_o}{r} \frac{e^{-jkR'}}{kR'} \right\} \quad , \tag{39}$$

where the minus sign in (39) is due to the fact that the image dipole is in the $-\hat{r}$ direction. Then, defining

$$E_{rr} = E_{rr}^{inc} + E_{rr}^{image} + E_{rr}^{dif} \quad , \tag{40}$$

we have

$$E_{rr}^{dif} = \frac{I\ell Z_o}{4\pi j} \left\{ \left(\frac{\partial^2}{\partial r_o^2} + k^2 \right) \frac{r_o}{r} \left(\pi^{dR} - \pi^{dR'} \right) \right\} \tag{41}$$

where π^{dR} and $\pi^{dR'}$ are defined in (16) and (17). Observe that when $\alpha<\pi/2$ there is no reflected E_{rr} field for $\phi>\pi/2$, so (41) does not strictly represent the diffracted field in the usual sense.

The source and image fields are then separated from the total field, and the $[Z_o]$ section of the total impedance matrix $[Z]$ is computed in closed form as before. The $[\Delta Z]$ elements are found by

$$\Delta Z_{ij} = - \int_{r_{oi}} \int_{r_j} I_i(r_o)\, E^{dif}_{rr}\,(r|r_o) I_j(r) dr\, dr_o, \qquad (42)$$

where r_{oi} ranges over the test mode and r_j ranges over the expansion mode. The differentiations in (41) can be eliminated by integration by parts, which also removes one of the integrations in (42). Note that, because of the non-zero wire radius, the electric field along the surface of the wire contains an E_θ component in addition to the E_r component. This E_θ component, which makes only a small contribution, has been ignored here.

This solution was programmed and run for a $\lambda/4$, $a=.001\lambda$ monopole, with a delta gap generator at the base of the monopole, vs angle α. Figure 10 shows Z_{in} using two modes on the wire compared with the surface patch MM solution. This result at $\alpha=\pi/2$ also agrees with the analysis for the vertical monopole in Section II as x_o approaches zero. Note that Z_{in} goes to zero as α approaches zero as expected, since the antenna then becomes shorted by the ground plane. As α approaches zero, the reactance curve takes a sharp turn downward before going to zero. This effect is probably explained by the fact that the capacitance between the monopole and half-plane increases sharply as the monopole gets closer to the half-plane, before going to zero as it touches the half-plane.

Another independent check is available from Tai[5] who computed the input resistance of a monopole at $\alpha=\pi$ by integrating the far field radiation pattern (the input reactance cannot be calculated using Tai's method). Also shown

in Figure 10 is a surface patch result obtained by Glisson[13] for a $\lambda/4$ monopole mounted on the edge of a finite plate, which compares reasonably with the other results.

The surface current density can be derived for a source at the edge of a half-plane in the same manner as was done in Section II. The final result for a dipole of moment $I\sqrt{\ell r_o}$ is

$$J_{sr} = \frac{-I}{\pi 2} \sqrt{\frac{\ell}{x}} \cdot \frac{1}{r} \sin \frac{\phi_o}{2} \text{ A/m} \quad . \tag{43}$$

The dipole moment must be reduced as $\sqrt{r_o}$ as $r_o \to 0$ to maintain finite fields. Note the correct source and edge singularities.

V. CONCLUSION

This paper has presented analysis and results of the problem of a monopole antenna mounted near or at the edge of a half-plane or plate. The canonical solutions using exact Green's functions have been presented as a basis for comparison with other solutions. Expressions for near-zone surface current density were derived and used to synthesize an attachment mode to handle wire attachments near plate edges in a general surface patch MM solution.

REFERENCES

1. F. M. Tesche and A. R. Neureuther, "The Analysis of Monopole Antennas Located on a Spherical Vehicle," IEEE-EMC-18, pp. 2-15, February 1976.
2. G. A. Thiele and T. H. Newhouse, "A Hybrid Technique for Combining Moment Methods with the Geometrical Theory of Diffraction," IEEE-AP-23, January 1975.
3. N. C. Albertsen, J. E. Hansen and N. E. Jensen, "Computation of Radiation from Wire Antennas on Conducting Bodies," IEEE-AP-22, pp. 200-206, March 1974.
4. E. H. Newman and D. M. Pozar, "Electromagnetic Modelling of Composite Wire and Surface Geometries," IEEE AP-26, pp. 784-789, November 1978.
5. C. T. Tai, "Dyadic Green's Functions in Electromagnetic Theory," Intext, Scranton, Pa., 1971, pp. 123-165.
6. Y. T. Lin and J. H. Richmond, "EM Modelling of Aircraft at Low Frequencies," IEEE AP-23, pp. 53-56, January 1975.
7. T. B. A. Senior, "The Diffraction of a Dipole Field by a Perfectly Conducting Half-Plane," Quart. Journ. Mech. and Applied Math., Vol. VI, Pt. 1, 1953.
8. J. H. Richmond, "Computer Program for Thin-Wire Structures in a Homogeneous Conducting Medium," Report 2902-12, August 1973, The Ohio State University ElectroScience Laboratory, Department of Electrical Engineering; prepared under Grant NGL 36-008-138 for National Aeronautics and Space Administration. (NASA-CR-2399)

9. P. Tulyathan and E. H. Newman, "The Circumferential Variation of the Axial Component of Current in Closely Spaced Thin-Wire Antennas," IEEE AP-27, pp. 46-50, January 1979.

10. R. G. Kouyoumjian and P. H. Pathak, "A Uniform Geometrical Theory of Diffraction for an Edge in a Perfectly Conducting Surface," IEEE Proceedings, November 1974, pp. 1448-1461.

11. E. P. Ekelman and G. A. Thiele, "A Hybrid Technique for Combining the Moment Method Treatment of Wire Antennas with the GTD for Curved Surfaces," Report 784372-5, July 1978, The Ohio State University Electro-Science Laboratory, Department of Electrical Engineering; prepared under Contract N00014-76-C-0573 for Office of Naval Research, pp. 48-55. OAD/A058495)

12. J. J. Bowman and T. B. A. Senior, "Diffraction of a Dipole Field by a Perfectly Conducting Half-Plane," Radio Science, vol. 2, No. 11, November, 1967, pp. 1339-1345.

13. A. W. Glisson, "On the Development of Numerical Techniques for Treating Arbitrarily-shaped Surfaces," Dissertation, University of Mississippi, June 1978.

14. D. R. Wilton and S. Govind, "Incorporation of Edge Conditions in Moment Method Solutions," IEEE AP-25, No. 6, November 1977.

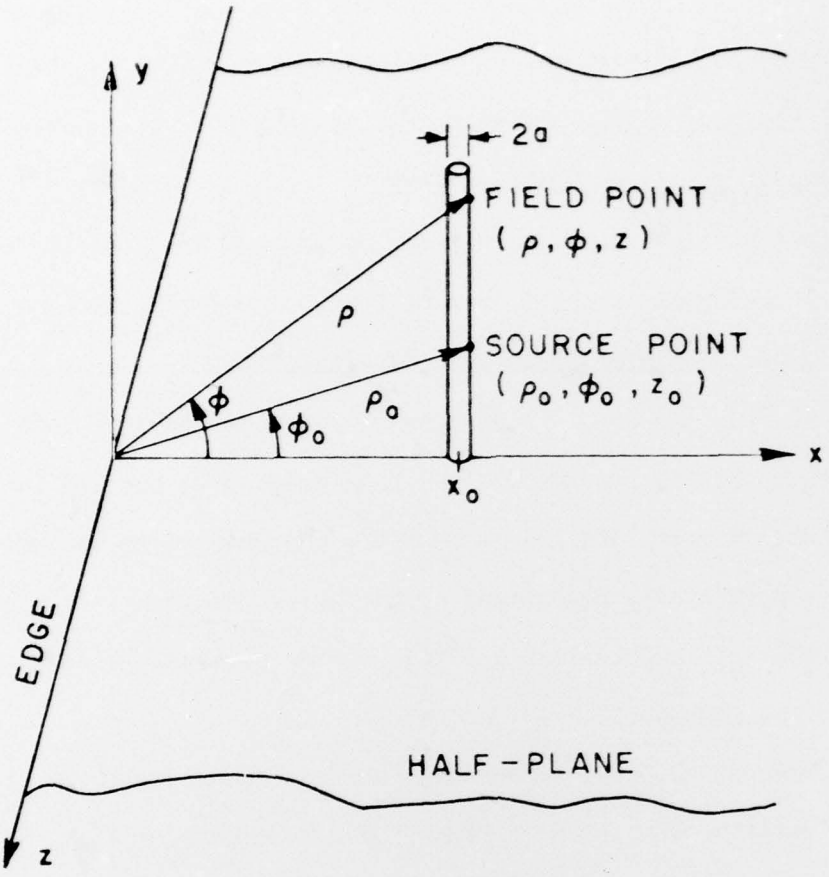

Figure 1. Geometry and coordinate system for a vertical monopole near the edge of a half-plane.

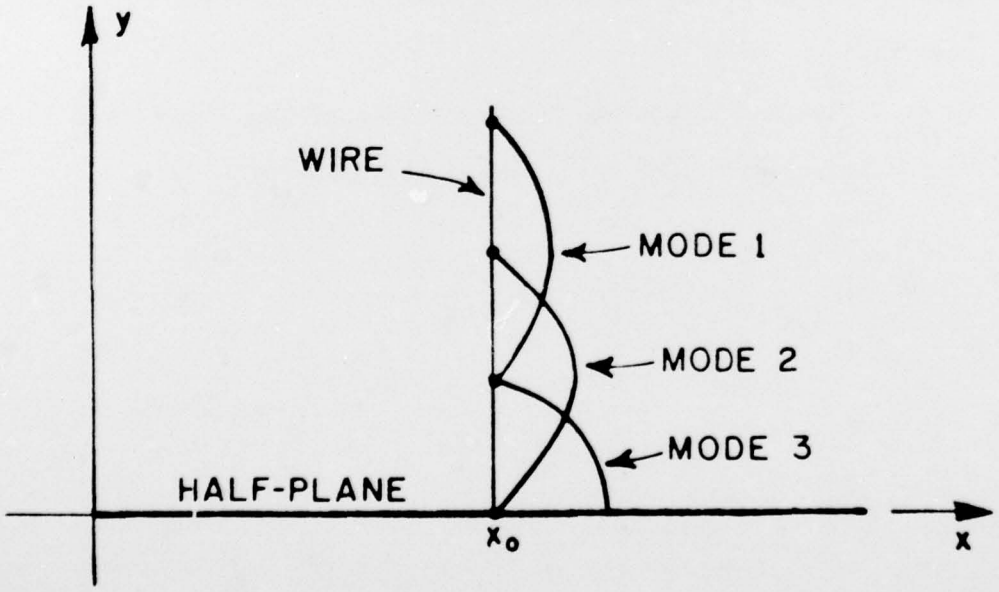

Figure 2. PWS expansion mode arrangement on wire.

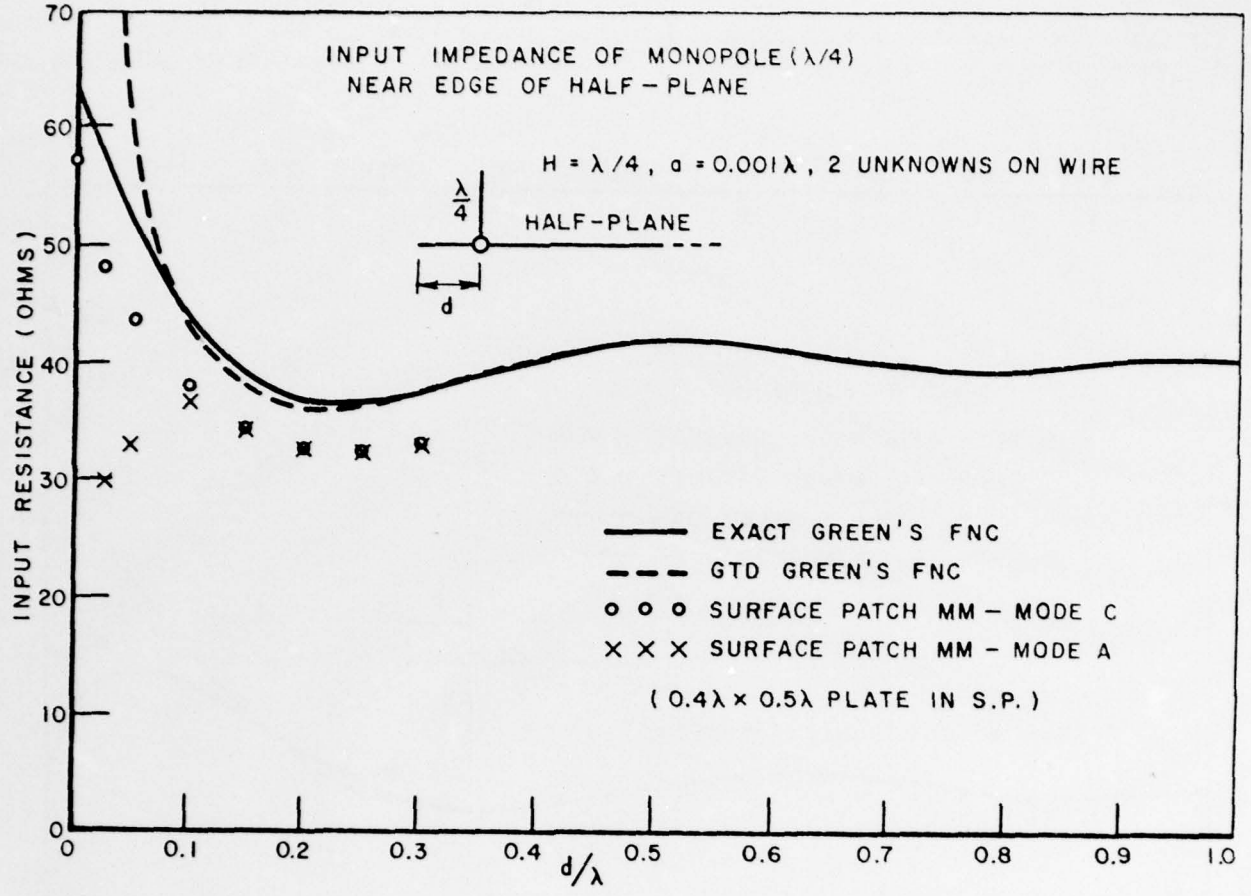

Figure 3. Input resistance of a λ/4 monopole vs. distance, d, from the edge of a half-plane computed using MM/exact Green's function, MM/GTD, surface patch with old att. mode (A), and surface patch with new att. mode (C).

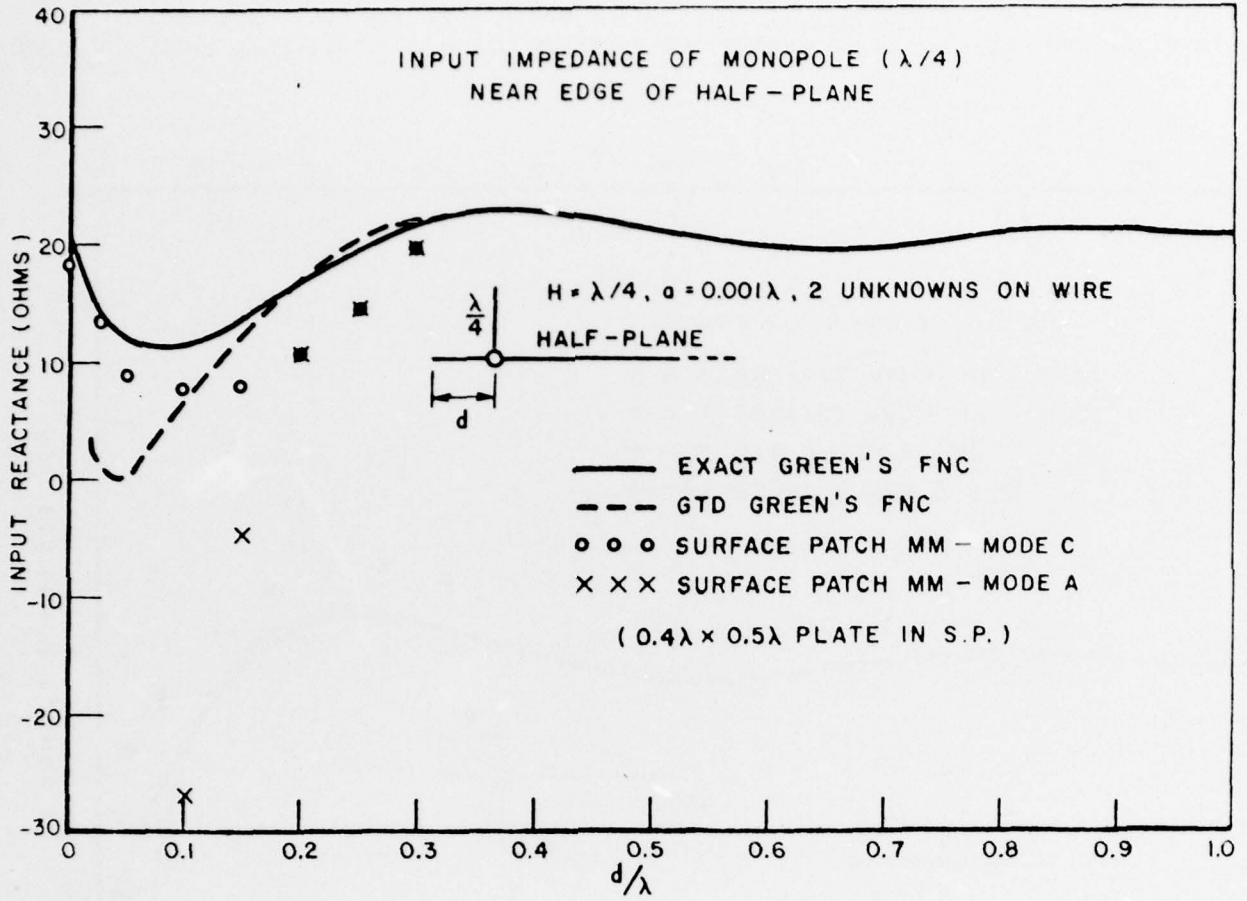

Figure 4. Input reactance of a λ/4 monopole vs. distance, d, from the edge of a half-plane computed using MM/exact Green's function, MM/GTD, surface patch with old att. mode (A), and surface patch with new att. mode (C).

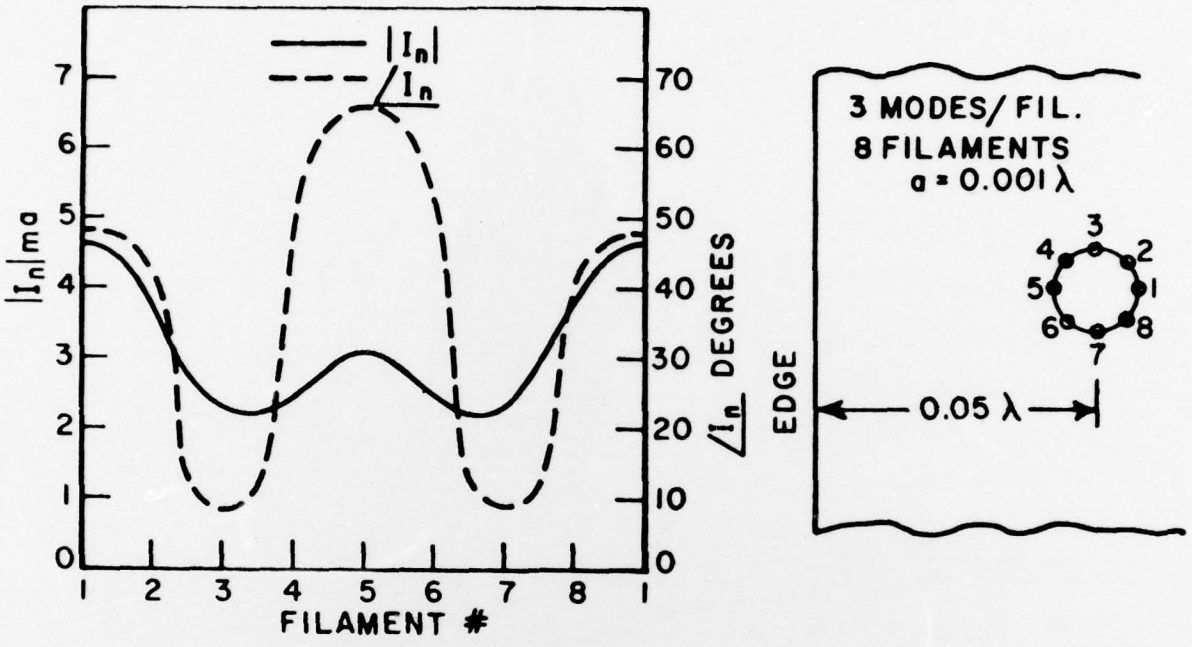

Figure 5. Magnitude and phase of filament current at the base of a monopole .05λ from a half-plane edge, vs. position around the wire. The layout of the eight expansion filaments is also shown.

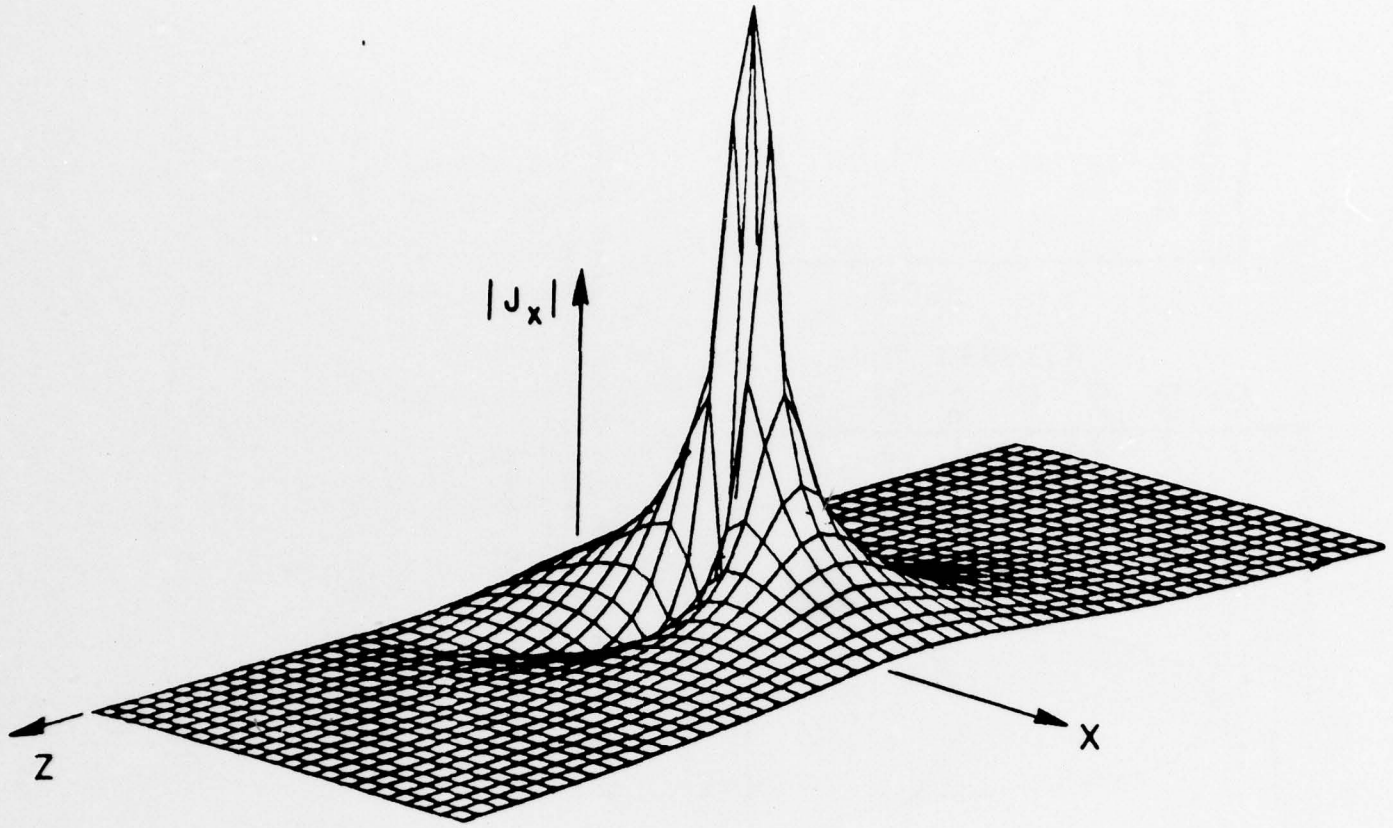

Figure 6. Three-dimensional plot of the magnitude of the surface current density J_{sx} (Equation (28)) for a vertical infinitesimal electric dipole .05λ from the edge of a half-plane. $.001\lambda \leq x \leq .1\lambda, -.125\lambda \leq z \leq .125\lambda$.

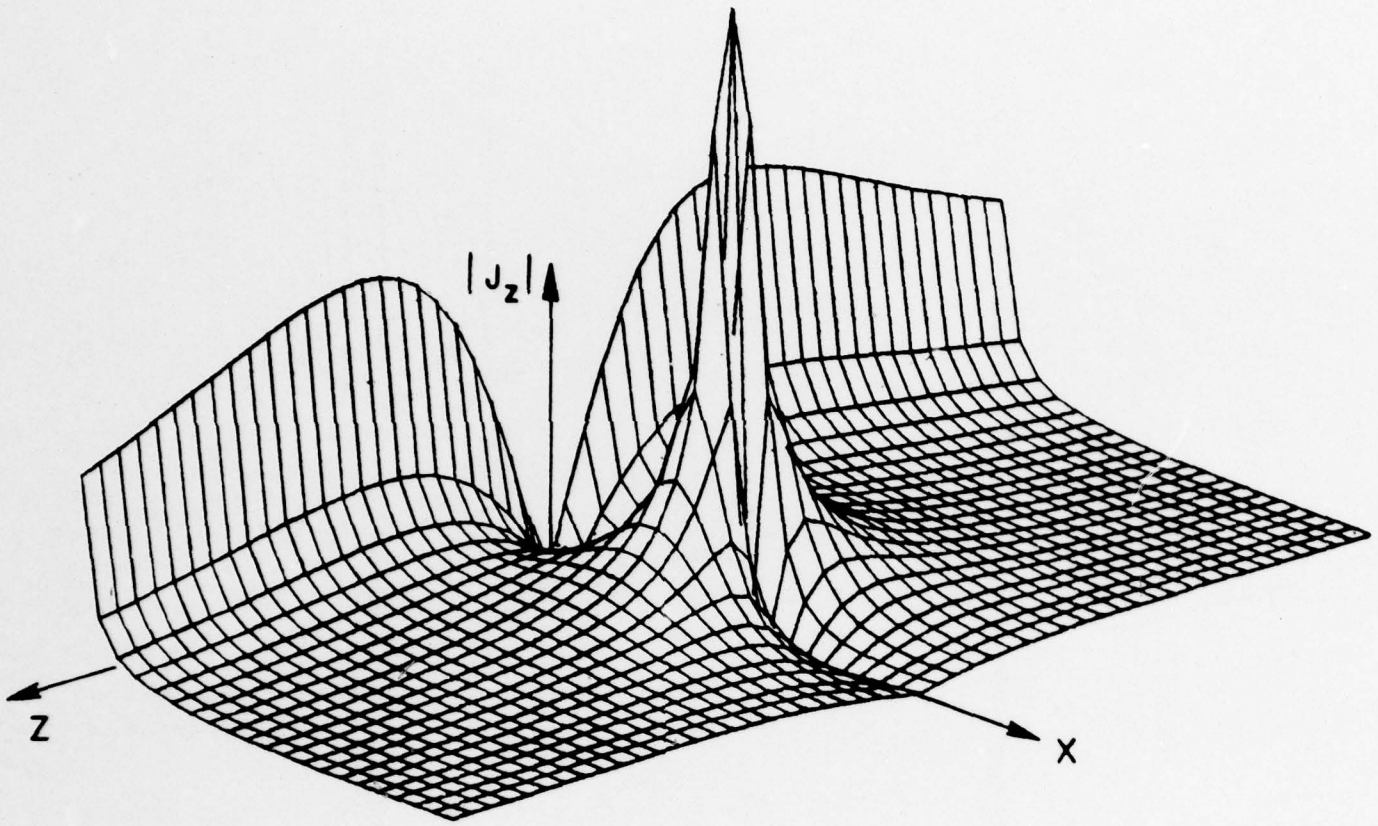

Figure 7. Three-dimensional plot of the magnitude of the surface-current density J_{sz} (Equation (29)) for a vertical infinitesimal electric dipole .05λ from the edge of a half-plane. $.001\lambda \leq x \leq .1\lambda, -.125\lambda \leq z \leq .125\lambda$.

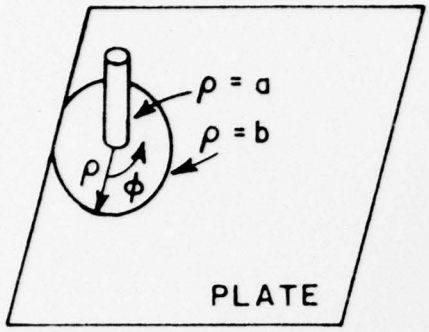

(a)

original attachment mode, mode A)

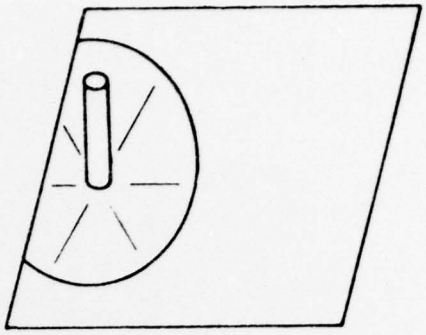

(b)

final attachment mode, mode C)

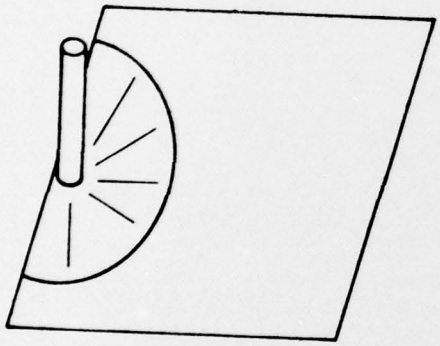

(c)

attachment mode C) when monopole is mounted at a plate edge.

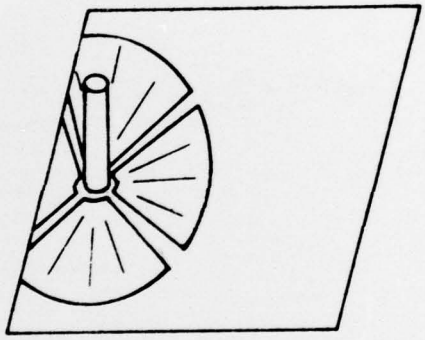

(d)

segmented attachment mode, mode D), shown with 4 segments.

Figure 3. Attachment mode development.

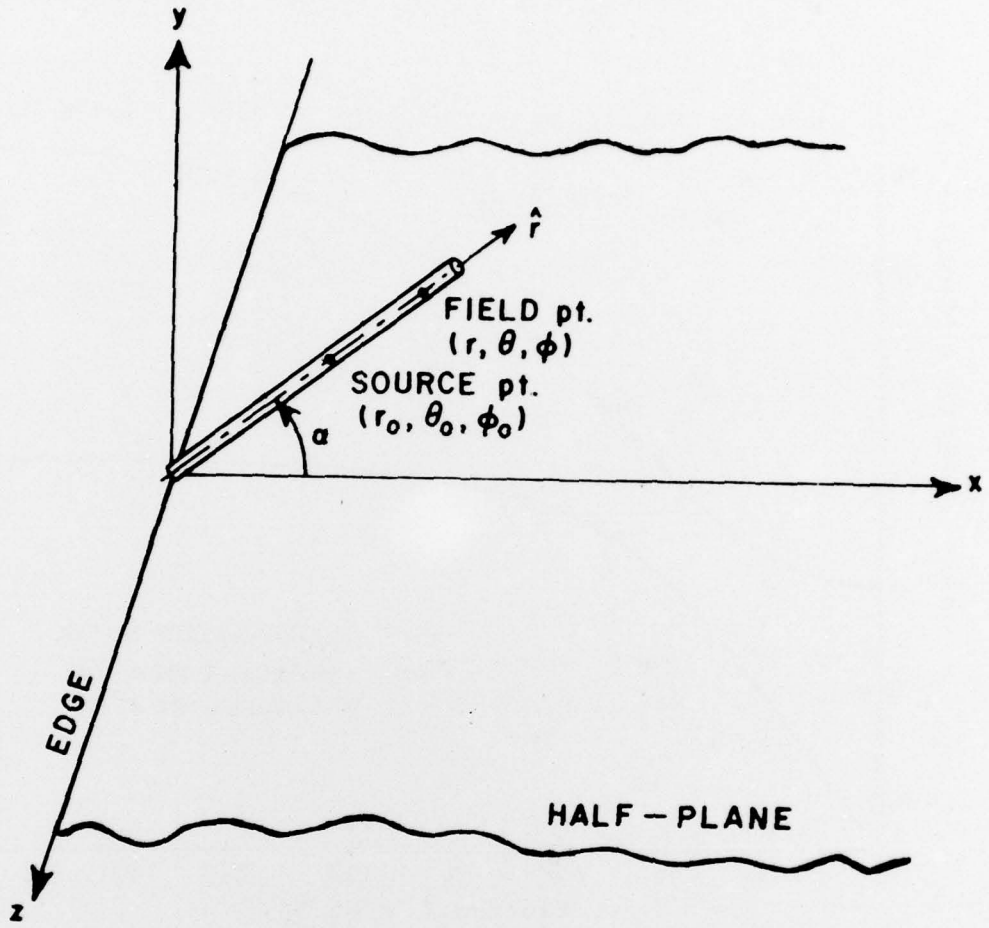

Figure 9. Geometry and coordinate system for a monopole mounted at the edge of a half-plane.

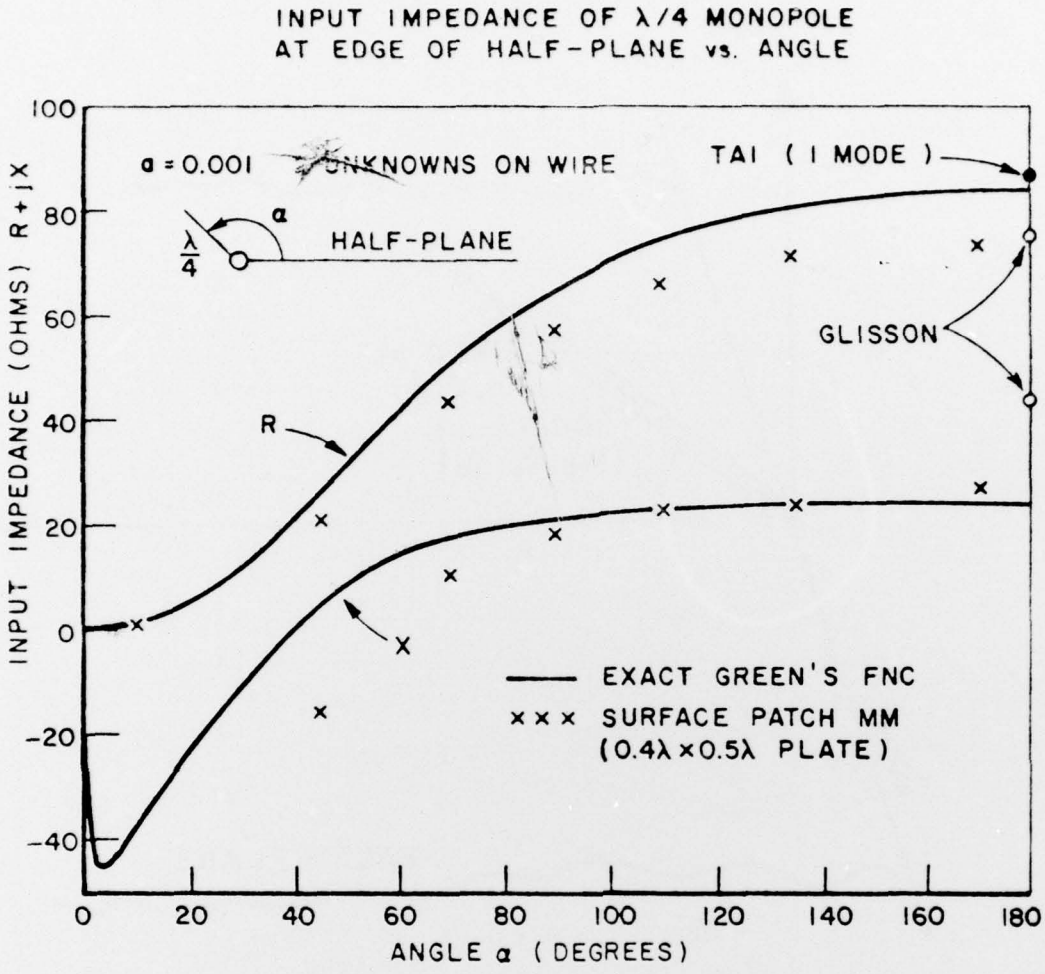

Figure 10. Input impedance of a λ/4 radial monopole mounted at the edge of a half-plane vs. angle, computed using MM/exact Green's function and surface patch with att. mode (C). Also shown are independent results for R and Z at $\alpha=180^{o}$, from Tai and Glisson, respectively.